

Study of the Influence of Substrate Shape and Roughness on Coating
Microstructure in Suspension Plasma Spray

Fernanda Caio

A Thesis

in

the Department

of

Mechanical, Industrial and Aerospace Engineering

Presented in Partial Fulfillment of the Requirements for the
Degree of Master of Applied Science (Mechanical Engineering) at
Concordia University
Montreal, Quebec, Canada

November 2017

© Fernanda Caio, 2017

CONCORDIA UNIVERSITY

School of Graduate Studies

This is to certify that the thesis prepared

By: Fernanda Caio

Entitled: Study of the Influence of Substrate Shape and Roughness on Coating Microstructure in Suspension Plasma Spray

and submitted in partial fulfillment of the requirements for the degree of

Master of Applied Science (Mechanical Engineering)

complies with the regulations of the University and meets the accepted standards with respect to originality and quality.

Signed by the final Examining Committee:

_____ Chair

Marius Paraschivoiu

_____ Examiner

Ali Dolatabadi

_____ Examiner

Saifur Rahaman

_____ Supervisor

Christian Moreau

Approved by

Chair of Department or Graduate Program Director

2017 _____

Dean of Faculty

Abstract

Study of the Influence of Substrate Shape and Roughness on Coating Microstructure in Suspension Plasma Spray

Fernanda Caio

Sprayed coatings produced with submicron particles have unique properties when compared to 10-100 micron particles. Suspension Plasma Spray (SPS) is used to deposit coatings from submicron particles. This process, which is a modification of the atmospheric plasma spray (APS) process, uses a liquid carrier to inject the fine particles into the plasma jet. However, this technique is still subject of extensive research efforts due to the complexity of the phenomena related to the liquid stream and the submicron particles in contact with the plasma jet. There is a wide range of parameters that affect the properties and microstructure of the coatings sprayed using SPS.

In this study, the influence of the substrate shape on the resulting coating microstructure is investigated. For this purpose, an yttria-stabilized zirconia (YSZ) suspension was sprayed on flat and curved stainless steel substrates by SPS. The suspension was composed of 20 wt.% YSZ particles in ethanol. After spraying, the morphology of the coatings has been characterized by scanning electron microscopy (SEM). The results showed that the substrate shape influences the amount of coating material deposited and column growth. The amount of coating material deposited was seen to decrease as the radius of curvature decreased. Finally, roughness influences the formation of columnar structure.

Acknowledgements

My sincere gratitude and appreciation to my supervisor, Dr. Christian Moreau, for the opportunity of performing this research in an exciting field of studies. Also, many thanks for all his patience, guidance and knowledge shared with me throughout these years.

My deep thankfulness to all the Concordia University Thermal Spray Laboratory group members for all the help and encouragement during my work. Special thanks to Dr. Fadhel Ben Ettouil and Alexandre Nascimento Romão for all the technical help during my experimental work.

Also, all my gratefulness to my family and boyfriend Nicolas, for their unconditional love and support. Without them, this accomplishment would have not been possible.

Table of Contents

1.	Introduction	1
1.1	Objective	3
1.2	Scope and limitations	4
1.3	Thesis outline	4
2.	Literature Review	5
2.1	Suspension Plasma Spray process.....	5
2.1.1	Origin of SPS.....	5
2.1.2	Description of the process	6
2.1.3	Suspension preparation	7
2.1.4	Injection of liquid	8
2.1.5	Plasma-liquid interaction	9
2.1.6	Coating formation.....	12
2.2	Coating microstructure characteristics	13
2.2.1	Coating morphology	13
2.2.2	Coating microstructure	14
2.2.3	Coating characterization	15
2.3	SPS process parameters effects on coating microstructure	16
2.3.1	Operating parameters.....	18
2.3.2	Suspension parameters	19
2.3.3	Substrate features.....	21
3.	Experimental Procedure	25
3.1	Substrate preparation	25
3.2	Suspension preparation	26
3.3	Spray process	28
3.4	Design of experiments	30
3.5	Coating characterization	31
4.	Results and Discussion.....	34
4.1	Results	34
4.1.1	Thin flat samples	34
4.1.2	Thin cylinder samples	38

4.1.3	Thin rod samples.....	42
4.1.4	Thick flat samples.....	47
4.1.5	Thick cylinder samples	50
4.1.6	Thick rod samples	55
4.2	Discussion.....	60
5.	Conclusions and Future work	65
	References	67

List of Figures:

Figure 1 - Schematic of a turbine blade and cross-section of the TBC multi-layers [3].....	2
Figure 2 - Micrographs of a TBC suspension plasma sprayed (left) and a micro conventional APS (right) [9]	3
Figure 3 - Schematic of SPS process [14]	6
Figure 4 - Schematic of liquid feedstock delivery [17].....	9
Figure 5 - Schematic of plasma jet zones [15]	10
Figure 6 - Evolution of a suspension droplet in the high temperature plasma [17].....	10
Figure 7 - Schematic of a typical impinging gas-jet system [23].....	11
Figure 8 - Schematic of particle trajectories within the hot gas flow and the respective coating [13].....	12
Figure 9 – Schematics of spray deposition characteristics with influence or not of substrate asperities: (a) 1SD, (b) 2SD and (c) 3SD [25].....	14
Figure 10 - Coating C1 (a) cross section and (b) top view [26]	14
Figure 11 - Coating C2 (a) cross section and (b) top view [26]	15
Figure 12 - Coating C3 (a) cross section and (b) top view [26]	15
Figure 13 - Schematic of SPS process parameters (Adapted from [14]).....	17
Figure 14 - Cross-sectional images of the as-sprayed coatings. Voids (P) and type II areas (II) marked [32]	20
Figure 15 - Schematic of radial injection of suspension into the plasma jet [33].....	21
Figure 16 - Plasma velocity contours for (a) flat and (b) curved substrates at different stand-off distances [37].....	22
Figure 17 - Plasma temperature contours for (a) flat and (b) curved substrates at different stand-off distances [37].....	23
Figure 18 - Samples: a) flat; b) cylinder; and c) rod	25
Figure 19 - Fixtures with samples: a) flat; b) cylinder; and c) rod.....	26
Figure 20 - Homemade suspension particle size distribution.....	28
Figure 21 - Schematic of the suspension injection into the plasma jet	29
Figure 22 - Thin Coarse Flat (4CF) cross-section and top view SEM images.....	35
Figure 23 - Thin Fine Flat (4FF) cross-section SEM images	36
Figure 24 - Thin Polished Flat (4PF) cross-section SEM images	36
Figure 25 - a) Thickness measured for Thin Flat samples, and b) variation of thickness for Thin Flat samples	37
Figure 26 - Roughness measured for Thin Flat samples	38
Figure 27 - Thin Coarse Cylinder (4CC) cross-section SEM images	39
Figure 28 - Thin Fine Cylinder (4FC) cross-section SEM images.....	40
Figure 29 - Thin Polished Cylinder (4PC) cross-section SEM images	41
Figure 30 - a) Thickness measured Thin Cylinder samples, and b) variation of thickness for Thin Cylinder samples	42
Figure 31 - a) Roughness measured for Thin Cylinder samples, and b) columns width measured for Thin Cylinder samples	42
Figure 32 - Thin Coarse Rod (4CR) cross-section SEM images	43
Figure 33 - Thin Fine Rod (4FR) cross-section SEM images.....	44
Figure 34 - Thin Polished Rod (4PR) cross-section SEM images	45

Figure 35 - a) Thickness measured for Thin Rod samples, and b) variation of thickness for Thin Rod samples	46
Figure 36 - a) Roughness measured for Thin Rod samples, and b) columns width measured for Thin Rod samples	47
Figure 37 - Thick Coarse Flat (TCF) cross-section SEM images	48
Figure 38 - Thick Fine Flat (TFF) cross-section SEM images	48
Figure 39 - Thick Polished Flat (TPF) cross-section SEM images.....	48
Figure 40 - a) Thickness measured for Thick Flat samples, and b) variation of thickness for Thick Flat samples	49
Figure 41 - a) Roughness measured for Thick Flat samples, and b) columns width measured for Thick Flat samples	50
Figure 42 - Thick Coarse Cylinder (TCC) cross-section SEM images.....	51
Figure 43 - Thick Fine Cylinder (TFC) cross-section SEM images	52
Figure 44 - Thick Polished Cylinder (TPC) cross-section SEM images	53
Figure 45 - a) Thickness measured for Thick Cylinder samples, and b) variation of thickness for Thick Cylinder samples	54
Figure 46 - a) roughness measured for Thick Cylinder samples, and b) columns width measured for Thick Cylinder samples	55
Figure 47 - Thick Coarse Rod (TCR) cross-section SEM images.....	56
Figure 48 - Thick Fine Rod (TFR) cross-section SEM images	57
Figure 49 - Thick Polished Rod (TPR) cross-section SEM images	58
Figure 50 - a) Thickness measured for Thick Rod samples, and b) variation of thickness for Thick Rod samples	59
Figure 51 - a) Roughness measured for Thick Rod samples, and b) columns width measured for Thick Rod samples	59
Figure 52 - Coating area in the cross-section of thick samples.....	61
Figure 53 - Particles trajectory in flat and cylinder samples [37]	62
Figure 54 - Alumina coating structure at stagnation point flow close to the torch exit: a) below the jet, b) at the center, and c) above plasma jet [38].....	63
Figure 55 - Digitized data for the substrate cross-section [39].....	63
Figure 56 - Micrograph of the coating in the over-sprayed area [39]	64
Figure 57 - Schematic curved substrate and particles possible trajectories before impact.....	64

List of Tables

Table 1 – Homemade suspension parameters	27
Table 2 – Plasma spray parameters	29
Table 3 – Design of experiments of samples sprayed.....	31
Table 4 – Thickness of Thin Flat samples in different positions	37
Table 5 – Thickness of Thin Cylinder samples in different positions	41
Table 6 – Thickness of Thin Rod samples in different positions	46
Table 7 – Thickness of Thick Flat samples in different positions	49
Table 8 – Thickness of Thick Cylinder samples in different positions.....	54
Table 9 – Thickness of Thick Rod samples in different positions.....	59

List of Equations

Equation (1) – Mass flow rate.....	9
Equation (2) – Stokes number.....	11
Equation (3) – Catch Rate.....	23

1. Introduction

In the last decades, the interest of the industry by thermally sprayed coatings has increased. Coatings are engineered solutions to modify and improve surface properties to desired levels of, for example, wear-resistance, thermal protection, corrosion-resistance, etc. Thermal spray processes can be customized and used to produce coatings with a variety of requirements. The applications of thermally sprayed coatings range from medical to aerospace industry, including printing, automotive, oil industries and more [1].

Nowadays, thermal barrier coatings (TBCs) in the aerospace industry are one of the main applications for suspension plasma spray (SPS) coatings. TBCs are used to protect and insulate metallic components from high operating temperatures in gas turbines for aerospace and energy generation applications. The thermal protection provided by TBCs makes it possible to increase combustion temperature and then the turbine efficiency. Moreover, it helps to limit the oxidation and to increase the component lifetime. TBCs are made from different materials in multi-layers called bond-coat layers and topcoat layer [2] [3].

The bond-coat layer acts as a protector from substrate oxidation and improves bonding with the topcoat. This layer is usually made by an oxidation-resistant metal. The topcoat consists of a ceramic material with low thermal conductivity, high coefficient of thermal expansion (CTE), in addition to high mechanical and chemical stabilities at high temperatures. The topcoat insulates the substrate from the heat due to its low thermal conductivity along with the microstructural voids, cracks and pores present [2] [3] [4] [5].

Yttria Stabilized Zirconia (YSZ) is highly used as a ceramic topcoat because its properties are suitable for topcoat requirements. YSZ melting point is around 2700 °C, and its thermal conductivity is one of the lowest of all ceramics at high temperatures [6]. Bernard et al. [5] have shown thermal conductivity of 0.7 W/mK at 1100 °C, in SPS coatings. The coefficient of thermal expansion of YSZ is $11 \times 10^{-6} \text{ K}^{-1}$ which it is high and close to the CTE of substrate super-alloy material typically used in TBCs, $14 \times 10^{-6} \text{ K}^{-1}$ [6].

Figure 1 shows a multi-layered TBC used in a turbine blade [2] [3] [4].

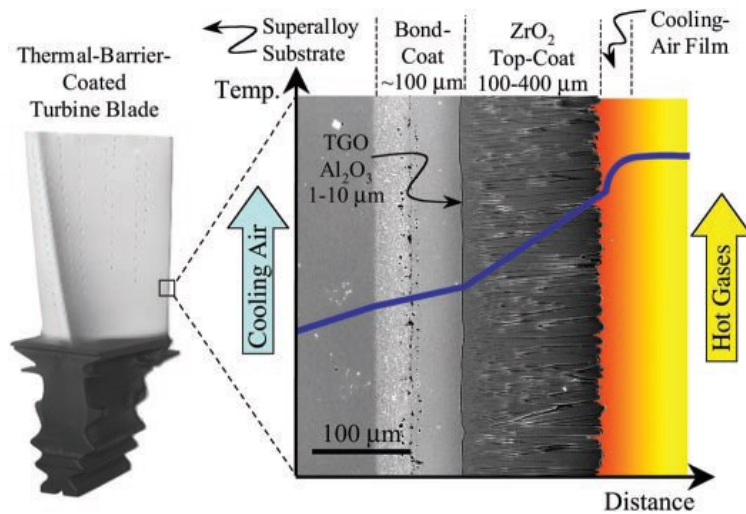


Figure 1 - Schematic of a turbine blade and cross-section of the TBC multi-layers [3]

Typically, two different methods were used to produce TBCs: atmospheric plasma spray (APS) and electron beam physical vapor deposition (EB-PVD). APS uses direct current plasma torch which forms a plasma jet from an electric arc and plasma gases flow. Small particles are injected to this plasma jet where they are accelerated and melted, finally impinging on the substrate. On the other hand, EB-PVD is a low pressure process. The deposition occurs under vacuum, where the coating is formed with the vapor of the coating material evaporated by focused high-energy electron beams [7].

EB-PVD produces coatings with columnar microstructure, which allows more thermal expansion and contraction comparing to APS coatings. However, it is also a more expensive process, and the coatings produced by EB-PVD are usually more thermally conductive than the others are. APS is a more flexible method and less costly, but the coatings produced by APS are likely to sinter, which reduces their mechanical and thermal properties [4] [8].

Recently, SPS started to be used to produce TBCs. SPS is a modification of APS process, using a liquid carrier to inject the nano-sized or submicron sized particles into the plasma jet. SPS process makes it possible to obtain coatings with vertical cracks, columnar or very porous structures. A reduced amount of micro-cracks can be observed in SPS coatings when compared to APS coatings (Figure 2). This happens because during the deposition in SPS, the splats are

thinner and the energy release rate during cooling tends to be lower. Thus, there is not enough energy for crack propagation [8] [9].

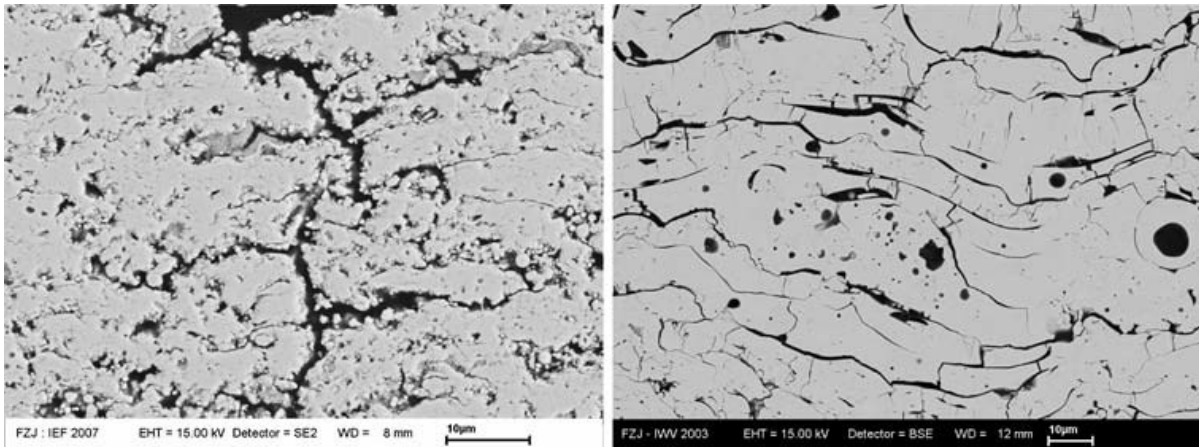


Figure 2 - Micrographs of a TBC suspension plasma sprayed (left) and a micro conventional APS (right) [9]

The microstructure of a SPS coating is desirable for TBC production because of its inter-columnar gaps and because of its nano-sized intra-columnar pores. Those characteristics help decreasing significantly the thermal conductivity of the coating and reducing thermal stresses during thermal cycling [10]. However, SPS is still the subject of many research due to the complexity of the phenomena related to the liquid stream and the sub-micron particles in contact with the plasma jet.

Important information on in-flight particles size, temperature and velocity are still missing in SPS. This makes it harder to understand how the coating microstructure is affected by changes in the parameters involved in the process. In an attempt to understand better how the substrate is influencing in the coating microstructure formation, the objective of this research was defined.

1.1 Objective

The objective of this research is to investigate the effect of the substrate curvature and roughness on SPS coatings microstructure. To do so, coating beads deposited on flat and curved substrates with different surface roughness were characterized. The beads were formed from multiple passages on the plasma torch on the same horizontal line. The importance of understanding how a more complex geometry can influence the coating microstructure was the driven force to perform this work. The plasma gases flow might follow different trajectories

depending on the shape of the substrate placed in front of it, affecting also the particles trajectories. As seen in Figure 1, the geometry of a real part to be coated usually has a more complex geometry than flat samples. Therefore, it is very important to understand how the geometry of the substrate influences on the coatings.

1.2 Scope and limitations

This work was performed with ceramic sub-micron particles (i.e. YSZ), typically used to produce TBCs. This material was chosen due to its high use by the aerospace industry. However, the work focused on the process of SPS itself, and not in a specific application.

The scope of this investigation is limited to the effects of the substrate features. The challenges of this work are the complexity and sensibility of the process. Additionally, the work is focused on the spraying of top coatings. Therefore, the bond-coats were not sprayed on the substrates, so the top coatings are applied directly to the surface of the substrates.

1.3 Thesis outline

This work was concerned with the effects of substrate characteristics (namely roughness and geometry) on the microstructure of coatings produced by SPS process. This thesis is divided in 5 chapters. A brief description of the chapters follows:

Chapter 1 presents the introduction to the work developed. The thesis is outlined and the objective is introduced. The scope and the limitations of this work are presented and explained. Chapter 2 brings the literature review related to the work done. First, TBCs are presented. Then, SPS process is described, followed by the coating microstructure features. The last section of Chapter 2 highlights some of the research done on this topic.

In Chapter 3, the experimental procedure is designed. The information on the experimental part of the work is detailed in this chapter. The experimental work preparation and strategy are described. Chapter 4 brings the results found with this work and discussion about the findings. The analyses of the coatings and the data extracted are presented. Some observations are made. Finally, the conclusions of the work and future research are stated in Chapter 5.

2. Literature Review

This chapter will describe SPS process and will present the coatings microstructure features. Additionally, recent research on SPS parameters will be highlighted. Furthermore, this literature review has been prepared in order to give an overview of the work done in SPS parameters, comparing them with the respective results on the coating microstructure.

2.1 Suspension Plasma Spray process

2.1.1 Origin of SPS

Starting in the mid-1990's, many studies have been done on nanostructured materials and finely structured coatings in the field of thermal spray technology. The interest for nanostructured materials has increased since they can provide advantages in engineering properties. The grain sizes are smaller than in micro-particles by almost two orders of magnitude [11]. Moreover, studies have shown that with a small grain-size, it is possible to get high-density nanostructured materials. For coating technology, this is very important and can bring advantages, mainly in plasma spray techniques [12].

The traditional plasma spray technique produces coatings with particles sized between 10 to 100 μm . These coatings can contain imperfections like un-melted particles, pores and cracks. These imperfections sometimes are desired for improving the coating function, for example, as in TBCs. The planar porosities, cracks and poor contact between lamellae in TBCs help to lower the thermal conductivity in YSZ, but also may decrease the life of the coating. Thus, the particles in the size range of 0.5 to 3 μm can produce coatings with small porosities and less micro cracks [12].

However, in the traditional plasma spray process it is not appropriate to inject powder with less than 5 μm of diameter. To do so, it would be necessary to increase significantly the carrier gas flow rate, which would perturb the plasma jet and the particles trajectory to the substrate. Additionally, there is the problem of fine powder clogging within the injection system. Different ways have been used to produce fine structured coatings and SPS technology is one of them. SPS

involves adding the sub-micron sized particles to be sprayed in a liquid medium, leading to the formation of a suspension that is injected in the plasma [12].

2.1.2 Description of the process

Plasma spraying process comprises a high intensity DC current arc between an anode and cathode which generates a plasma jet within a plasma torch. The plasma gas injected in the torch is heated by the arc and exits the nozzle as a plasma jet with high temperature and velocity [7]. This high velocity flow is necessary to accelerate the fine particles injected into the plasma jet, so they can impinge on the substrate [13]. The injection of the particles can be axial or radial, through an internal or external injection system. The schematics of SPS process with radial injection is shown in Figure 3 [14].

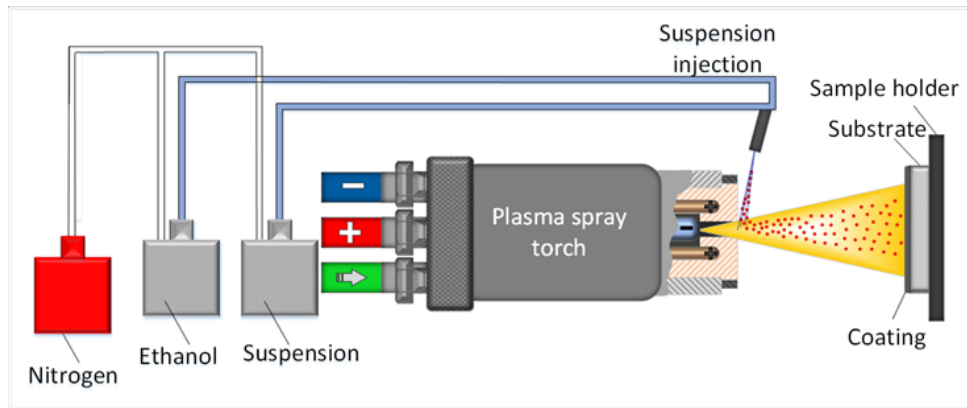


Figure 3 - Schematic of SPS process [14]

Different types of plasma torch can be used for SPS, such as conventional, triplex or axial injection torches. Conventional plasma torches that use stick-type cathodes, work in a power range of 20 to 60 kW with plasma gases mixtures of Ar-H₂, Ar-He or Ar-H₂-He. This torch produces a 40 to 50 mm plasma jet core length, and typically, with high voltage fluctuations. In order to limit these fluctuations, none or a small content of H₂ should be used [12] [15].

Triplex torches have three cathodes and three electric sources, producing three parallel arcs attached to a single anode. Using an Ar-He gas mixture, it is possible to reach 100 to 120 V with a plasma jet core of 55 to 60 mm of length. Furthermore, the axial injection torch has three cathodes and three anodes operated by three independent power supplies. The mean arc voltage

can be up to 120 V with the plasma jet converging within an interchangeable nozzle and the suspension injected axially in the middle of the three plasma jets [13] [15].

The distance between the torch and the substrate being coated is called standoff distance. For different applications or spray parameters adjustments, there is a different optimal standoff distance. The spray or surface speed is the relative speed between the torch gun and the substrate being coated [7] [16].

SPS process comprises these steps: suspension preparation, injection of liquids into the jet, plasma-liquid interaction and coating build up [17]. The suspension may enter in the spray system on the form of liquid jet or spray of drops. The injection can be done by pressurizing the liquid with air or gas to enter in a tube that takes it to the injection location [18].

The following physical phenomena are involved in SPS process [19]:

- Injection of the liquid (suspension) into the plasma jet.
- Primary fragmentation, or breakup, of the liquid stream and secondary breakup of the droplets.
- Vaporization of the liquid.
- Acceleration, heating and melting of the sub-micron sized particles.
- Potential agglomeration and/or occasional evaporation of the fine particles.
- Impact, spreading and solidification of the particles on the substrate.

These multiphase phenomena happen in a small space and a very short period of time (a few centimeters and a few milliseconds) [19].

2.1.3 Suspension preparation

A suspension can be described as a heterogeneous mixture of liquids and solids [18]. The principal component is the solvent which can be organic or water. The most commonly used in SPS are ethanol and water [11]. Besides the liquid and the sub-micron sized particles, some other elements, as dispersing and stabilizing agents, can also be added to the suspension. This is to improve the rheological properties, avoid or reduce the agglomeration of the particles and their sedimentation [17] [20].

According to Pawlowski [17] there are some properties that have to be controlled to spray a suspension in the thermal spray system:

- Dispersion and stability: suspension has to be dispersed and stable for the duration of the process. The fine particles suspended should not agglomerate.
- Sedimentation: particles should not sediment in the bottom of the container due to gravity during the processing time.
- Viscosity: related to injection mechanism. Depends on injector and tube size.
- Interaction with jet/flame: solvent makes a difference in contact with plasma jet: water cools it down and ethanol heats it up [17].

The suspension has to be fed in a controlled way and has to be transported with no interruptions to the torch through a calibrated nozzle [17].

2.1.4 Injection of liquid

There are two different ways to inject the liquid into the plasma flow: atomization or full liquid jet, known as mechanical injection [13]. Depending on which system is used, the liquid could be entered in the plasma flow in form of liquid stream, drops or droplets [21].

Atomizer systems produce droplets with an extensive size distribution and spray angles. This angle could get up to 60°. The external dimensions of the atomizers are around 20 or 30 mm, which complicates the injection of the droplets close to the torch nozzle exit. The size distribution of the droplets should be as narrow as possible in order to control the interaction of the droplets with the plasma jet. Additionally, it is necessary to adapt the droplet velocity for the penetration into the hot gas jet [13].

In mechanical injection, the suspension can be transported to the spray system by pressurized vessel or by peristaltic pump. The suspension is stored in a pressurized reservoir and forced through a stainless steel injector, with a nozzle of internal diameter varying from 50 to 300 μm . The suspension can be injected into the plasma plume as a liquid jet that is atomized by the high-speed plasma, or it can be atomized before the injection. Figure 4 shows the schematic of the pressurized reservoir [11] [17] [20].

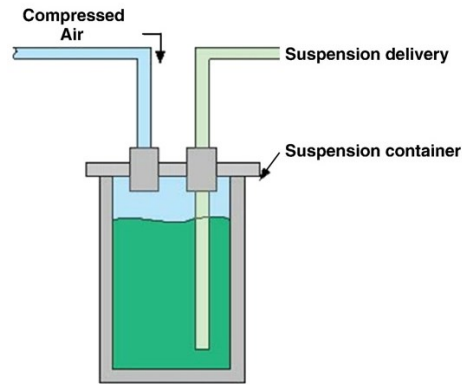


Figure 4 - Schematic of liquid feedstock delivery [17]

Using the pressurized vessel system, it is possible to control the injection velocity by controlling the pressure of the gas. The mass flow rate (m_l) is expressed as follows (Equation (1)), where ρ_l and v_l are, respectively, the liquid specific mass and average velocity at the injector exit, and d_n is the injector internal diameter [11].

$$m_l = \rho_l \times v_l \times \frac{\pi d_n^2}{4} \quad (1)$$

2.1.5 Plasma-liquid interaction

Within the plasma jet, there are three major areas: plasma jet core, plasma plume and plasma fringe.

Figure 5 shows the schematic of these major areas, called zones 1, 2 and 3. In the plasma jet core (Zone 1), the injected liquid will cross the highest heat and momentum transfer area, with temperatures above 8000 K. The plasma plume (Zone 2) is the area where the heat and momentum transfer capabilities will be decreased when comparing with plasma core. The temperature will vary from 3000 to 6000 K [11] [15].

Finally, in the plasma fringe (Zone 3), the momentum will be high enough to fragment the liquid stream but the heat treatment on the droplet will not be sufficient. It would be ideal if all the droplets of the suspension could be injected directly into the plasma core area. Therefore, it is very important to inject the liquid as close as possible to the torch nozzle exit [11].

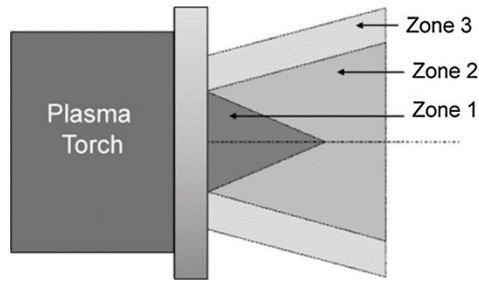


Figure 5 - Schematic of plasma jet zones [15]

When the suspension is injected into the system, the droplets are accelerated in the plasma jet and the liquid evaporates from the droplet. Thus, the fine particles get in direct contact with the hot gas. Figure 6 shows the behavior of a droplet when interacts with the plasma jet [17].

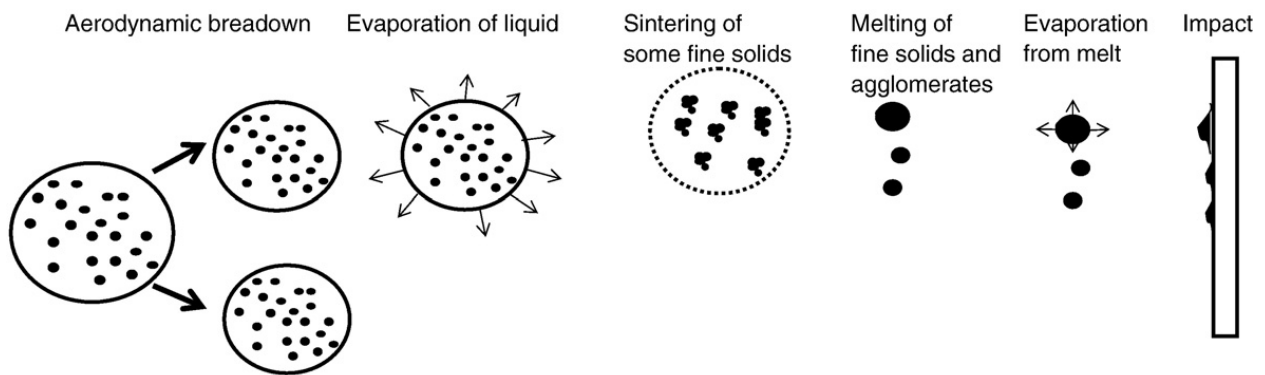


Figure 6 - Evolution of a suspension droplet in the high temperature plasma [17]

The big droplets from the suspension enter into the high speed plasma jet. The drag force between them produces shear deformation in the droplets. This phenomenon is called aerodynamic breakup, and it happens right after the injection of the droplets into the plasma jet [17]. However, if the injection process feeds the liquid in a form of a liquid stream, a primary breakup may occur. This is caused by the plasma cross flow. Thus, the droplets resulting from the first breakup may go through a second breakup [21].

After the aerodynamic breakup, the suspension liquid is evaporated from the small droplets in the phase called evaporation of liquid. Subsequently, the sintering process of fine particles occurs with the agglomeration of fine particles into greater particles. Next phase, the fine particles and the sintered agglomerate are melted. Some evaporation can occasionally occur. Finally, the particles impinge on the substrate [17].

Furthermore, in the impact phase, the fine particles with low inertia will possibly be advected by the flow, following trajectories parallel to the surface of the substrate, not impacting on it. Unlike those fine particles, the ones with higher inertia will continue on their initial trajectory and will impinge on the substrate [22]. These happens because of an impinging jet system shown in Figure 7 [23].

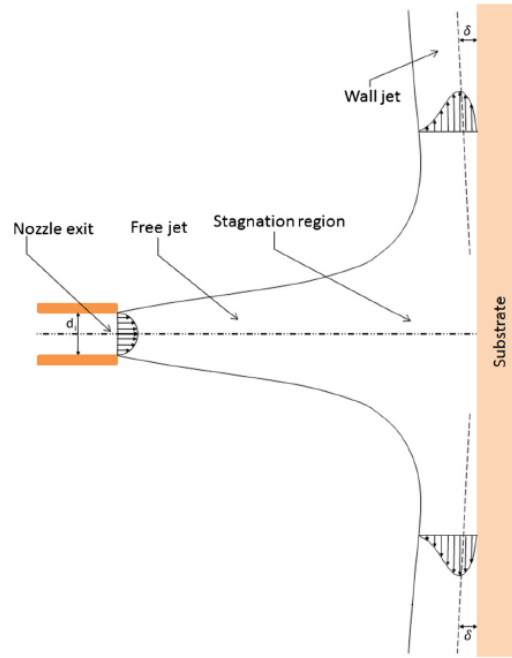


Figure 7 - Schematic of a typical impinging gas-jet system [23]

It is possible to see in Figure 7 that in the stagnation region the flow turns and moves laterally parallel to surface of the substrate. This is because the gas axial velocity decreases and the static pressure on the substrate increases, as the plasma gas gets closer to the substrate. Stokes number can be used to study the gas-particle interaction and the particles trajectory close to the substrate. Stokes number is given as follows (Equation (2)) [23]:

$$St = \frac{\rho_p d_p^2 v_p}{\mu_g l_{BL}} \quad (2)$$

Stokes number is the ratio of particles inertia and the fluid drag on the particle where ρ_p is particle density, d_p is particle diameter, v_p is particle velocity, μ is the gas viscosity and l_{BL} is the

thickness of the flow boundary layer in front of the substrate. Particles with low Stokes number will follow the gases flow. On the other hand, particles with high Stokes number will follow their trajectory to the substrate being less affected by the gases flow [15] [23].

2.1.6 Coating formation

The sprayed particles getting to the substrate, or to the previously deposited coating layer, can be found on the substrate in one of the three following conditions [11]:

- Those that have been well treated. These particles were fully molten and form lamellae when impacting and spreading on the substrate.
- Those that have traveled in the jet fringe area and are in a powdered state.
- Those that have been molten and re-solidified. These particles might be expelled to plasma jet cooler areas when they are subjected to turbulence or thermophoresis effect. Thermophoresis effect takes place when fine particles come across high temperature gradients during their trajectory [13].

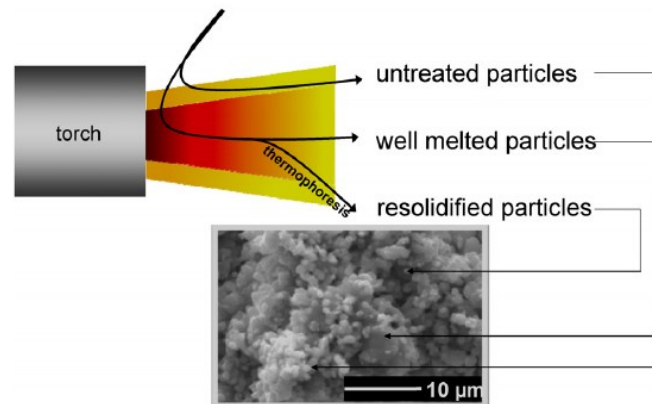


Figure 8 - Schematic of particle trajectories within the hot gas flow and the respective coating [13]

Figure 8 shows the schematic of particle trajectories within the hot gas flow and the respective result in the coating [13]. The molten particles deform and solidify fast once they impinge on the substrate, forming lamellae. The two main shapes of lamellas are: pancake, in the form of a deformed disk, which are shaped from particles of low thermal and/or kinetic energy; or flower, a splashed particle with a corona with dendrites around [17] [20].

2.2 Coating microstructure characteristics

As already described in the previous section, SPS coatings have lamellae, unmolten particles, molten and re-solidified particles and voids. These features pile up layer by layer of spray passes [17]. Studies have shown that SPS process can produce highly porous coatings, as well as dense, columnar type or vertical cracked coatings [24].

2.2.1 Coating morphology

According to Fauchais et al. [12], suspension plasma sprayed coating morphologies are related to the fragmentation of the drops and the penetration of droplets into the plasma jet. Due to the nature of the process, in each bead deposited, the center of the spraying jet is denser and more adherent. However, in the fringes, the particles are more powdery and not so adherent.

Therefore, with bead overlapping, the powdery phase is covered with a denser phase in the next bead. Furthermore, some material might be vaporized and re-condensed when impacting to the substrate, or previous coating layer, contributing to defects within the coating. These phenomena occur in the entire coating build up, bead by bead, pass by pass [12].

VanEvery et al. [25] categorized the spray deposition microstructure development in three types: 1SD, 2SD and 3SD. Type 1 spray deposition (1SD), forms coatings with inter-deposit gaps that produce columnar structures. This happens because of the inertia difference between suspension droplets and plasma. This makes some droplets to be unable to follow the plasma direction and impact on the sides of the surface asperities. Figure 9 (a) shows the schematic of deposition characteristics for 1SD.

Type 2 of spray deposition (2SD) has more droplets than 1SD. These droplets follow trajectories to impinge in substrate asperities shadowing the surroundings of the asperities as suggested in Figure 9 (b). This behavior is called *shadowing effect*. Lastly, in type 3 of spray deposition (3SD), the plasma drag forces do not interfere in the deposition of the particles. Thus, in 3SD the deposition occurs on the surface and asperities, without shadowing from the asperities (Figure 9 (c)) [25].

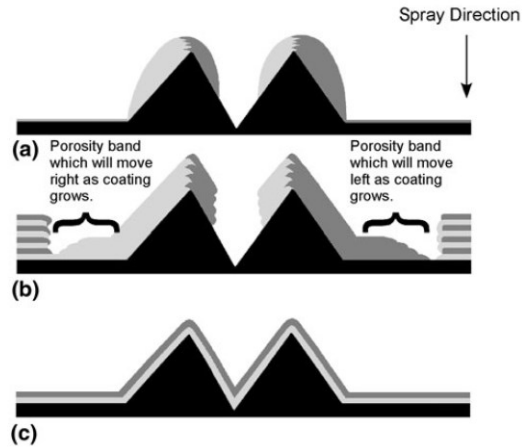


Figure 9 – Schematics of spray deposition characteristics with influence or not of substrate asperities: (a) 1SD, (b) 2SD and (c) 3SD [25]

2.2.2 Coating microstructure

Depending on spray parameters and resulting droplet size, velocity, temperature and trajectory different coating microstructures are produced. For example, Ganvir et al. (2015) [26] have identified three different coatings (C1, C2 and C3). These coatings were produced by axial SPS varying the spray parameters in order to get different microstructures. All the coatings were sprayed with Axial III plasma gun (Northwest Mettech Corp., Canada).

The suspension used was 25 wt.% of 8YSZ in ethanol. YSZ particle size distribution was $D_{50} = 490$ nm. Plasma gases Ar, H₂ and N₂ formed the gas flow used. Figure 10 shows the cross section and top view of coating C1. It is a porous coating with some column formation. Coating C2 (Figure 11) showed a microstructure in a feathery columnar-type. Finally, coating C3 showed a microstructure with vertical cracks and inter-pass porosity bands as shown in Figure 12 [26].

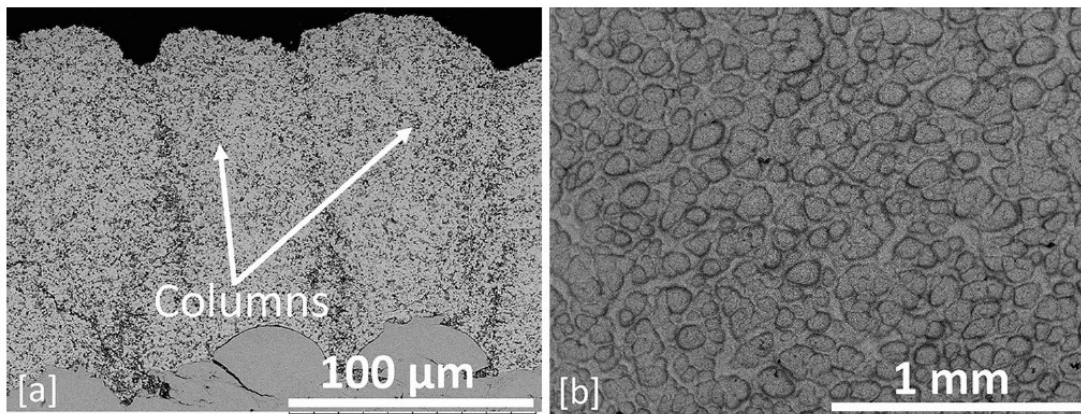


Figure 10 - Coating C1 (a) cross section and (b) top view [26]

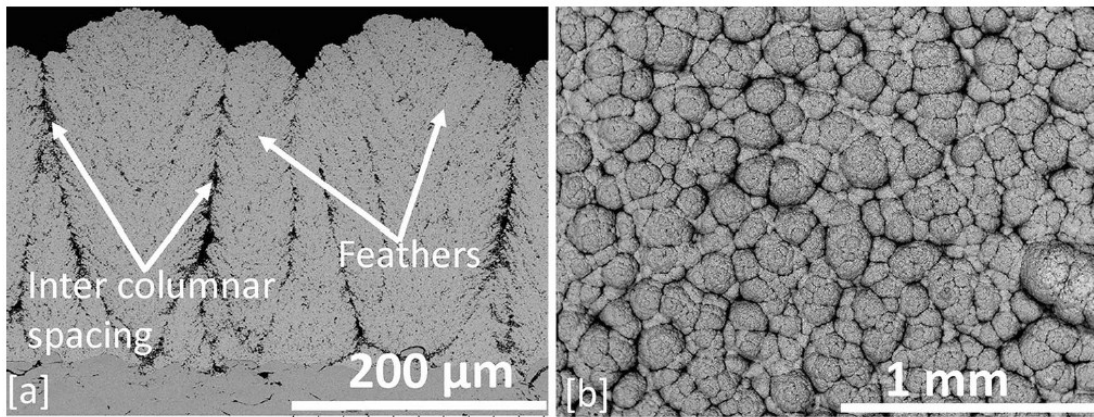


Figure 11 - Coating C2 (a) cross section and (b) top view [26]

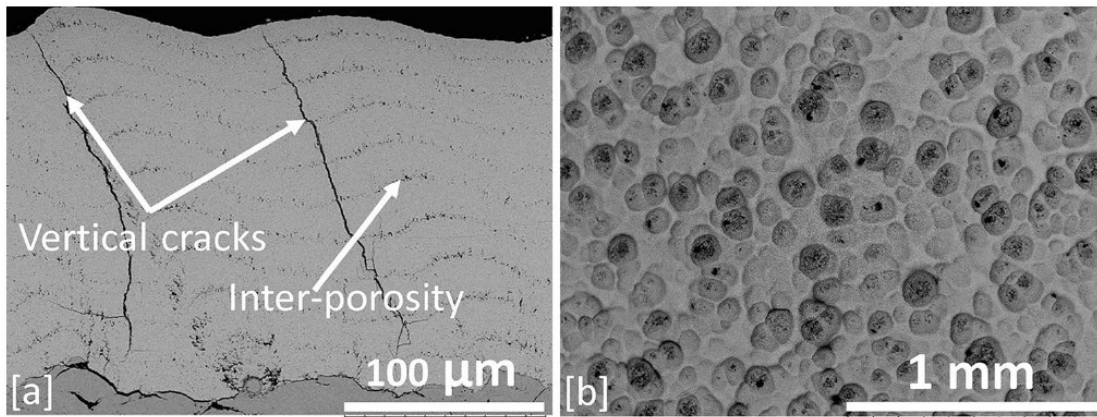


Figure 12 - Coating C3 (a) cross section and (b) top view [26]

2.2.3 Coating characterization

By means of testing and characterization methods, it is possible to understand how the coating is expected to behave in working conditions. Thermal, mechanical and adhesion-cohesion are examples of properties that can be identified by testing and characterization methods [7].

These methods are important to evaluate the usefulness of the coatings. Research has been done in order to understand and develop appropriate techniques for testing coatings. Even though thermal sprayed coatings are different from processed bulk materials, some common techniques have been imitated from other material science disciplines, for example, metallography and image analysis [27].

Microstructure analyses can be done in the cross-section of the coatings or on the surface (top view). The cross-section shows the inside of the coating, for instance pores, cracks and lamellae structures. The top view reveals the outside part of the coating. Metallographic preparation of the substrate area of interest is done before image analysis observation [28].

The first step in metallographic preparation is sectioning of sample. Following, the sectioned sample is impregnated in a low-viscosity resin and cured. The last steps are grinding and polishing the sample impregnated, in order to get a mirrored surface. After the preparation, the microstructure observation can be performed with Optical Microscopy (OM), or Scanning Electron Microscopy (SEM) for higher magnification, for example [28].

Coating characterization is very important to understand what happens during spraying. Consequently, intensive research has been done on comparing coatings produced from different spray parameters. Significant research effort has been put by both industry and academia in order to understand the relationship between spray parameters and coating microstructure. In the following section some of these research will be highlighted.

2.3 SPS process parameters effects on coating microstructure

The properties and microstructure of the coatings produced by SPS depend on a large number of process parameters. Figure 13 shows a schematic of SPS process and parameters that can influence the coating microstructure:

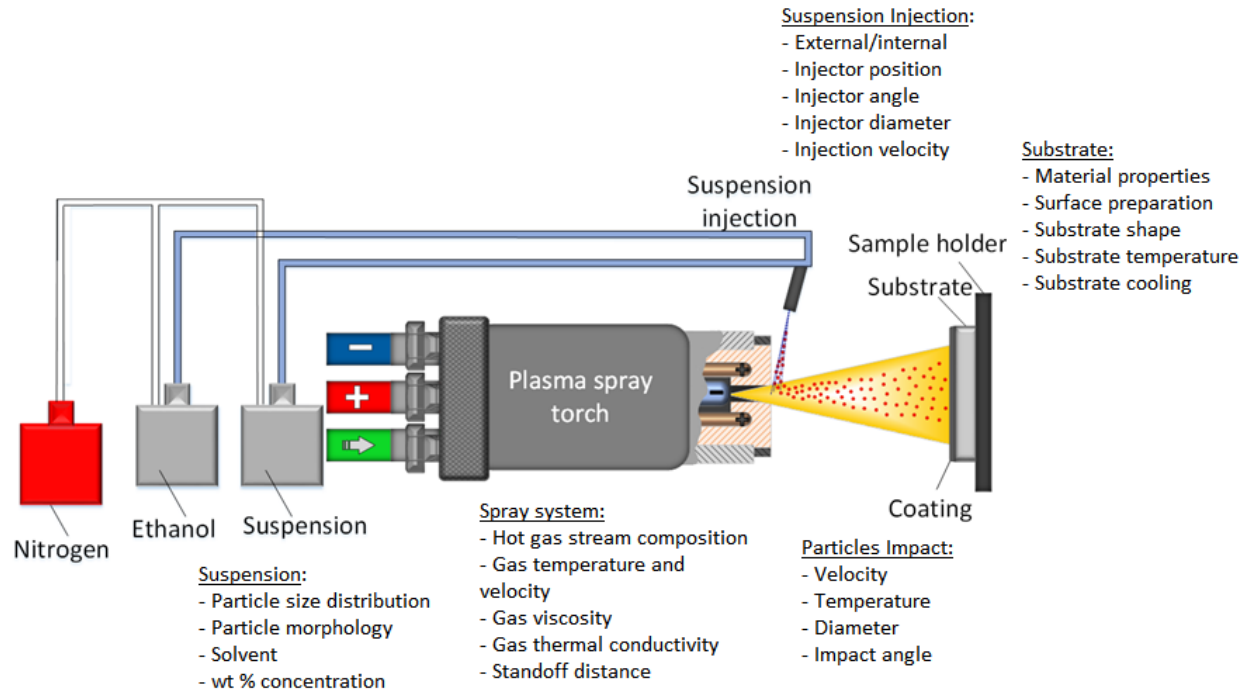


Figure 13 - Schematic of SPS process parameters (Adapted from [14])

As shown in Figure 13, for each component of the process, such as suspension or its injection, spray system and substrate, there are many parameters that can be changed and play a role in forming the microstructure of the coating. For each application, the parameters have to be meticulously chosen and adjusted to produce the coating desired.

As mentioned before, one of the differences between APS and SPS is that in APS process the coatings are built by micrometer-sized particles, while in SPS the coatings are produced by sub-micron and nanometer-sized particles. Therefore, the mechanisms to control the coating formation are different. In the plasma phase, due to their low inertia, the liquid feedstock and the fine particles are very sensitive to the instantaneous characteristics of the plasma jet and their variations [22].

The SPS process requires control of many parameters and extensive research has been dedicated on understanding the relationship between them and the coating microstructure. Numerical modeling have been significantly helping in understanding the phenomena involved in SPS. Since methods of measuring in-flight particles velocity, temperature and diameter in SPS are not completely developed until now, modeling results validated by the experimental ones

have given a closer perspective of what is happening. This section will highlight the experimental and numerical research done on SPS parameters.

2.3.1 Operating parameters

Several studies have been carried out on plasma spray operating parameters in the last decades. The research done on spray parameters have tested different plasma guns, inputs on power supply, different plasma gases and flow rates, spraying velocities and stand-off distances. The findings include porosity as related to torch power and stand-off distance, coating microstructure with cracks related to plasma jet instability and substrate temperature during spraying.

In the study carried out by Joulia et al. [22], different conditions were tested to spray YSZ coatings with fully homogeneous microstructure by SPS. The results of this study showed that the key points in order to achieve a fully homogeneous microstructure without vertical cracks and particle stacking defects are the stability of the plasma jet, the control of the temperature of the substrate during spray and control of the particles trajectories close to the substrate.

Gas mixtures of argon and helium or argon with less than 5 vol. % hydrogen could be used to get stable plasma jets. Additionally, an increase on the helium content resulted on an increase on the plasma jet enthalpy and velocity which provides a better heat treatment for the particles in the jet [22].

Furthermore, in the study performed by Macwan et al. [29] YSZ coatings were sprayed with three different standoff distances and three torch power. The microstructure analysis of the coatings showed pores, unmelted or partially melted particles and micro-cracks. It was observed that porosity is closely related to torch power and standoff distance. The coating with the highest porosity was produced with the lowest torch power. Moreover, the smaller the stand-off distance and the higher torch power, the denser the coating was.

Meillot et al. [30] performed a numerical analysis by modeling different plasma flows interactions with liquid injection. The simulations showed different liquid trajectories and breakup modes. Their results showed that the interaction between fluids, i. e. plasma flow and liquid jet, can be described by the Weber number. The Weber number of a gas is the ratio of the

disrupting aerodynamic forces to the restorative surface tension force. The simulations were validated by comparing results with breakup mechanisms for the same Weber number in the plasma cross-flow, at constant temperature [30].

2.3.2 Suspension parameters

Studies have been done analyzing the effects of the suspension parameters and its injection on the coating microstructure and properties. The suspension parameters that have been studied are, for example, the suspension composition, comprising the powder that has been used, the particle size of the powder, the solvent, and the solid load of powder in the suspension. The injection of the suspension has also been object of study. Some of the conclusions showed that the suspension composition is related to coating microstructure and performance.

Curry et al. [31] varied suspension parameters to understand the influence of the suspensions on the coatings microstructure and mechanical properties. The conclusion of this study showed that one can produce particular coating microstructure and performance by choosing the suspension composition. Suspensions with ethanol as solvent were seen to be more likely to form coatings with columnar microstructure when suspension viscosity is decreased. This can be achieved by stronger atomization and consequently formation of smaller particles in the plasma jet plume [31].

They have also observed that when using water as the suspension solvent, the microstructure have changed from columnar to vertically-cracked. Additionally, with water as the solvent, they observed that the suspension has a higher surface tension. This alteration was found to increase the thermal conductivity and decreases the thermo-cyclic fatigue life. Finally, they have concluded that the median powder particle size in suspension does not have a direct influence on the coating deposition type. In other words, the powder size itself is not enough to define parameters for spraying the coatings [31].

Carpio et al. [32] studied the effect of the particle size distribution of the suspension feedstock on the microstructure of SPS YSZ coatings. The findings of this study showed that all the coatings presented a microstructure with two zones, one with fully melted areas (I) and the other with sintered grain areas (II), as showed in Figure 14.

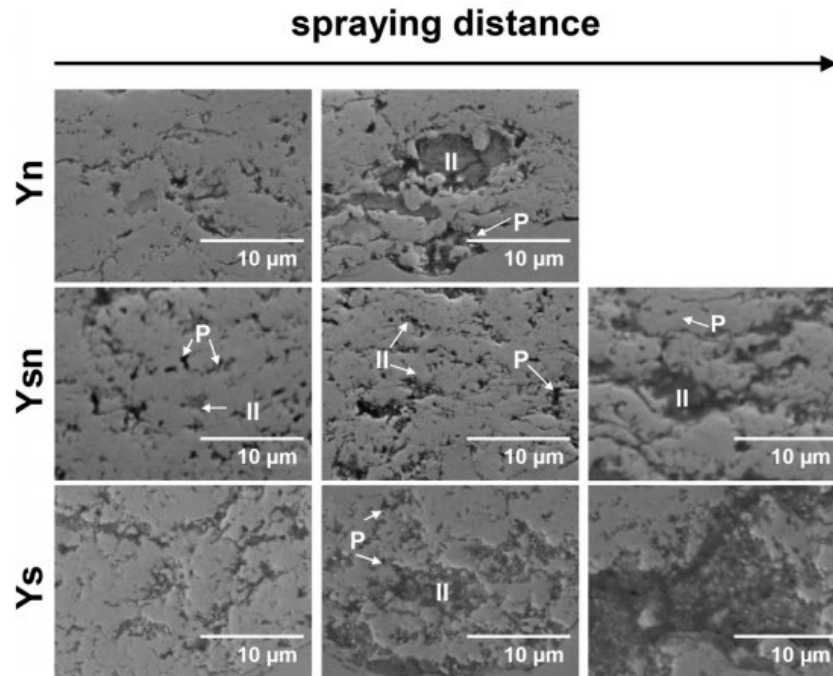


Figure 14 - Cross-sectional images of the as-sprayed coatings. Voids (P) and type II areas (II) marked [32]

In the same study, it was observed that increasing the standoff distance, the porosity increases as well as the partially melted areas. At constant spraying distance, the partially melted areas increased as the suspension particle size changed from sub-micron to nanosized particles. The mechanical properties decreased as the stand-off distance increased. Finally, the mixture of nano and submicron-sized particles in the suspension can give balanced results between suspension processability and final coating [32].

A numerical study performed by Jabbari et al. [33] found that the suspension penetration depth depends on its injection velocity. Increasing the suspension injection velocity will lead to a higher penetration depth, up to a certain point. After that point, a reduction in number of the molten particles will occur. Additionally, porosity was found to increase if the standoff distance increases, and the particles' temperature and velocity were the highest at a standoff distance of 4 cm. Finally, the velocity and temperature of fine particles and the suspension penetration depth are higher when the injector is close to the nozzle exit and it is positioned towards the gun, as shown in Figure 15 [33].

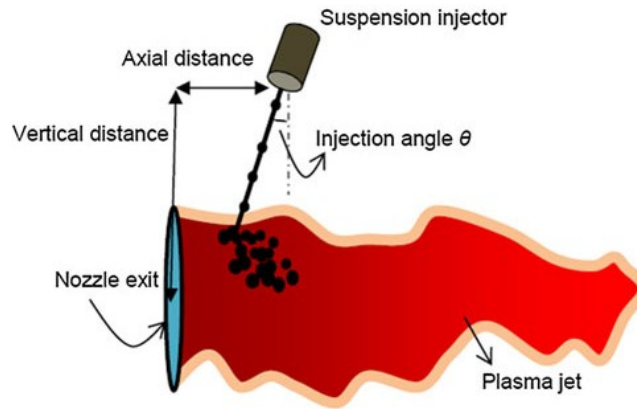


Figure 15 - Schematic of radial injection of suspension into the plasma jet [33]

2.3.3 Substrate features

Studies have shown that substrate surface topography influences the microstructure of the coating and the substrate shape interferes on the trajectory and velocity of the particles close to it.

Curry et al. [34] studied the influence of the surface topography of bond coats on the structure of SPS coatings. Some APS bond coats with modified surface roughness by polishing and grit blasting, in addition to as sprayed APS and HVOF bond coats were sprayed by SPS. The results showed that the surface topography of the substrate does influence in producing columnar microstructure in SPS coatings. It was observed that as the bond coat roughness increased, the columns formed in the SPS coating developed in a more asymmetrical way and were wider. The authors suggested that, in principle, controlling the surface topography of the substrate could partially design the SPS coating microstructure [34].

Sokolowski et al. [35] [36] performed a more complete study focused on the microscopic analysis and characterization of TBC's with different microstructures. Different parameters were tested to better understand which are the most appropriate to produce each different coating microstructure. Coatings were sprayed with two different plasma torches, the suspensions composition had two different powders and several fractions of solid content, in addition to four different surface preparation techniques [36].

Studies were carried out to characterize the coatings with different microstructures. The conclusion of this study showed that porosity and topography of coatings are related to the solid

weight composition and powder particle size in the suspensions. Lower concentration of powder and smaller particle size produced coatings with columnar microstructure. Plasma torch also influences the coating microstructure. Using different torches was possible to create different microstructures, such as more homogeneous coatings or more flexibility to spray different coatings [36].

Pourang et al. [37] studied the effect of the substrate curvature on in-flight particle temperature, velocity and trajectory through a three dimensional numerical analysis. Figure 16 and Figure 17 show the modelling results for plasma temperature and velocity.

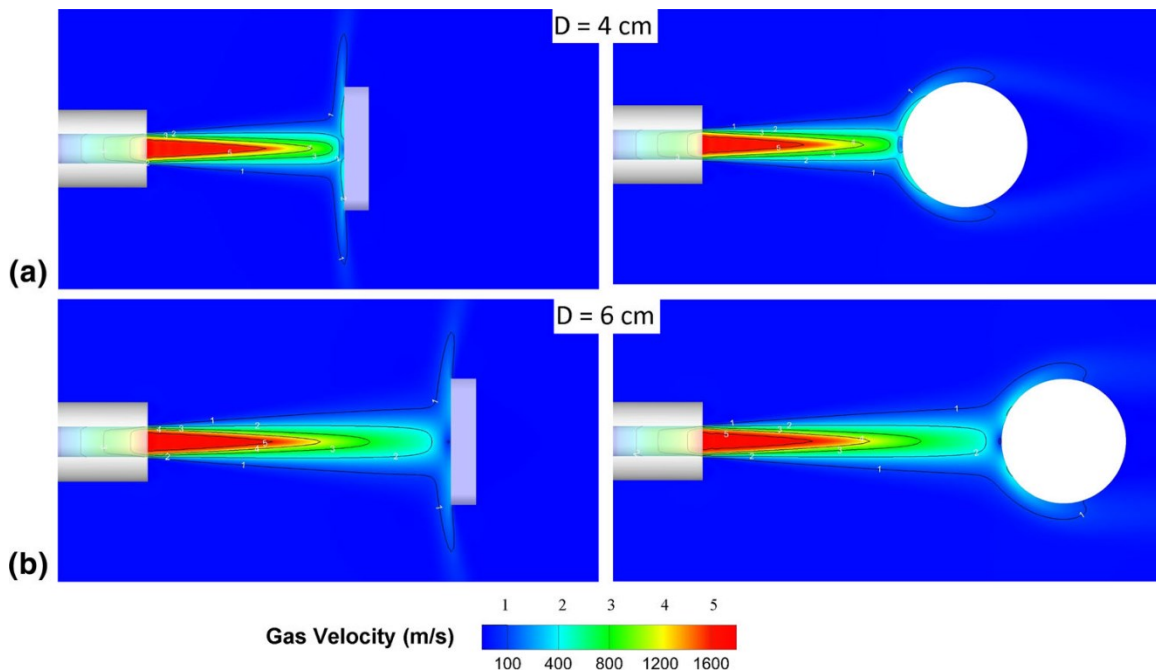


Figure 16 - Plasma velocity contours for (a) flat and (b) curved substrates at different stand-off distances [37]

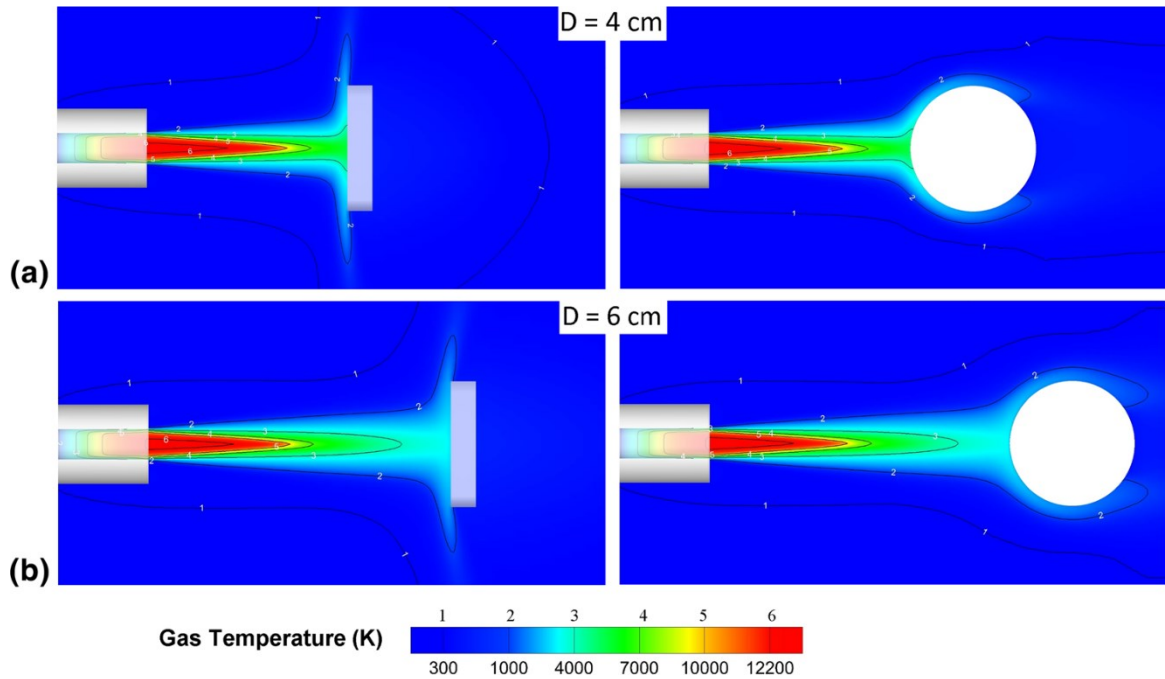


Figure 17 - Plasma temperature contours for (a) flat and (b) curved substrates at different stand-off distances [37]

After a quantitative analysis, they have observed that the particles impinge on the flat substrate about 2.2 times more often than on the curved, for a fixed time interval. With this observation, the parameter “Catch Rate” was defined by the equation (3):

$$\text{Catch Rate (\%)} = \frac{\text{mass of landed particles in } \Delta t}{\text{mass of injected particles in } \Delta t} \times 100 \quad (3)$$

The conclusion of this study showed that the substrate and its shape have an important influence on the trajectory and the velocity of the particles close to the substrate. The catch rate for the flat substrate was found much higher than on the curved one, which resulted also in a lower amount of coating deposited on the curve substrate. It was observed also, that the majority of the particles reach the curved substrate at angles of 10° up to 20° , and above this value, the particles will pass over the surface without impinging on it. Furthermore, once again the standoff distance was observed and a shorter distance was shown to produce higher deposition [37].

As the research highlighted in this chapter shows, the sensitivity of the process is very high. Any changes in the parameters can produce different coatings. This research was also used as benchmarking in order to decide the parameters used in this work.

Furthermore, there is not much effort been put in understanding the effects of the shape of the substrate. This was the motivation of the work. As already showed, Pourang et al. [37] did some modelling on particles behavior having different substrate shapes. Their simulation study was the inspiration for this experimental work, observing the effects on the coatings microstructure. In the next chapter, the experimental procedures of this work will be explained.

3. Experimental Procedure

This chapter describes in details the experimental procedure followed in this work. Coatings were sprayed on substrates with different shapes. All the spray parameters used and the experiments are explained in the following sections.

3.1 Substrate preparation

The substrate material of the samples used in this work was stainless steel 304. Three different shapes were chosen in order to analyze how the substrate curvature affects the coating microstructure. Firstly, the flat squared sample (dimensions 2.54 cm x 2.54 cm x 0.3 cm) and the cylinder sample (dimensions 2.54 cm of length, 2.54 cm of external diameter and 0.3 cm wall size) were sprayed. After that, the rod sample (dimensions 15 cm of length and 0.8 cm of external diameter) was added to the experimental work (Figure 18).

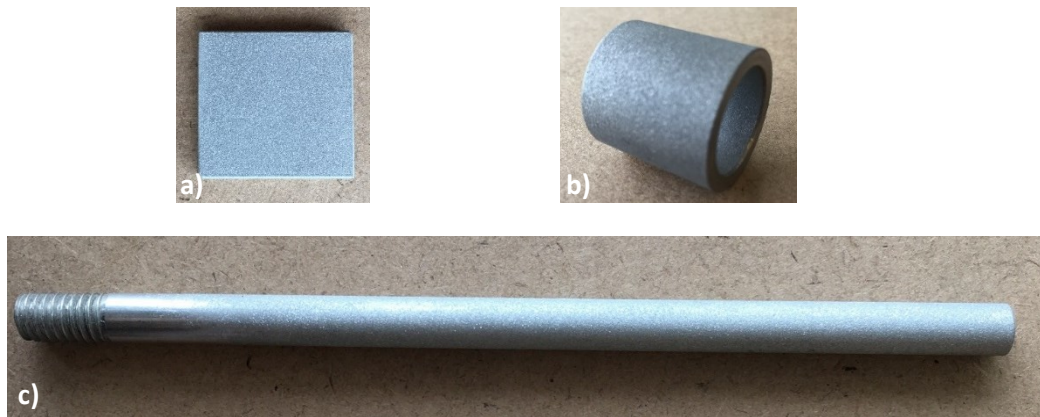


Figure 18 - Samples: a) flat; b) cylinder; and c) rod

The substrates received three different surface treatments. The substrates denominated “polished” were machined in order to have a roughness close to $Ra = 0.1 \mu\text{m}$. For the three shapes, the substrates were also grit blasted with aluminum oxide (Al_2O_3), producing other two different surface roughness, $Ra \approx 2 \mu\text{m}$, denominated as “fine”; and $Ra \approx 5 \mu\text{m}$, denominated as “coarse”. The roughness was measured with a profilometer (Mitutoyo, Japan) in the center of the samples, in the same orientation of the scanning of the plasma torch.

All samples were cleaned in alcohol and dried by blowing compressed air. After that, the samples were fixed to the sample holders, as shown in Figure 19.



a) Flat samples and holder



b) Cylinder samples and holder



c) Rod sample and holder

Figure 19 - Fixtures with samples: a) flat; b) cylinder; and c) rod

Once the samples were placed on the sample holder, the latter was fixed to the table inside the spray booth, ready to be sprayed.

3.2 Suspension preparation

The suspension used in this work was made by the author, in the Thermal Spray Laboratory (TSL), with the characteristics shown in Table 1. Those characteristics were chosen based on the research done and the resources available in the laboratory. The powder was YSZ (Zhonglong Chemical, China) with ethanol as the solvent, in order to get a better deposition efficiency. The particle size distribution used was sub-micron size and the solid concentration of powder was chosen based on the torch power available in the TSL.

Table 1 – Homemade suspension parameters

Solvent:	Ethanol
Powder:	Yttria Stabilized Zirconia (YSZ)
Particle size distribution:	d(50) = 400 nm
YSZ solid content:	20 wt.%
Dispersant:	Polyvinylpyrrolidone (PVP)
PVP solid content:	1 wt.%

The suspension preparation started by drying the YSZ powder in a furnace at 120 °C during one hour. Then the ethanol was poured into a glass container and the PVP gradually added to it. The mix of ethanol and PVP was stirred by magnetic agitation, which helped in dissolving the particles in the solvent. After having a homogeneous mix of ethanol and PVP, the YSZ powder was gradually added to the mix. In order to help particles suspend in the solvent and decrease agglomeration, an ultrasonic agitator was used during this process. All the suspension components were weighted with a high precision scale to have the accurate proportion of 80% solvent and 20% powder.

Once all the powder was put into the solvent, the suspension was introduced to the injection reservoir. The injection system consists of two sealed pressurized reservoirs. One contains the suspension to be sprayed with a mechanical stirrer, and the other contains water. A compressed gas pressurizes the tanks and mechanically injects the suspension through the hoses up to the injector into the plasma jet. In this work, the gas inserted was argon with a pressure of 50 psi and the injector was made of stainless steel with an internal diameter of 150 µm, having an injection feed rate of around 21 mL/min.

The suspension particle size distribution was measured with Spraytec device. The particles measurement results were $D_{10} = 0.204 \mu\text{m}$, $D_{50} = 0.414 \mu\text{m}$ and $D_{90} = 0.814 \mu\text{m}$ and the distribution graph is shown in Figure 20:

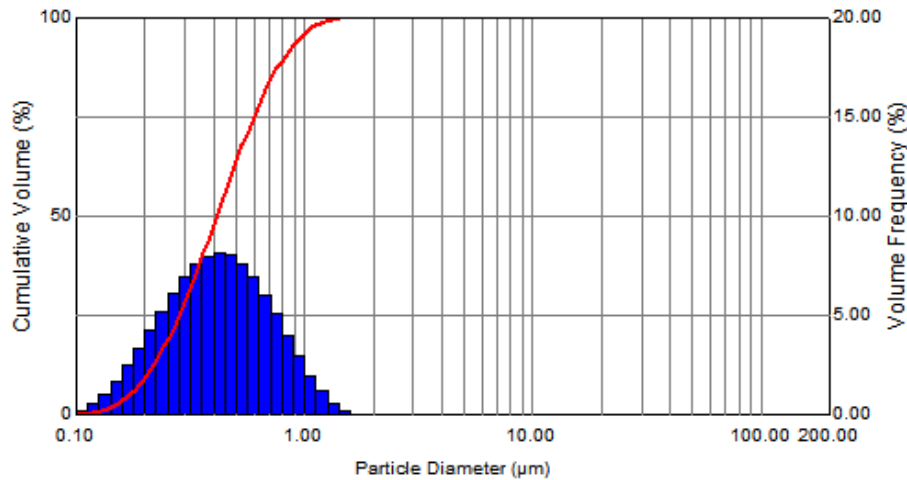
Particle Size Distribution

May 25 2017 - 17:19:37

Fernanda-2017-05-25-YSZ-ethanol.smeal\Exp 001 - May 25 2017\May24-test1 1 1.psd

Sample : May24-test1

Start+1:32 (s)



Size (µm)	% V <	% V	Size (µm)	% V <	% V	Size (µm)	% V <	% V
0.112	0.18	0.18	1.12	98.02	1.99	11.22	100.00	0.00
0.126	0.69	0.52	1.26	99.20	1.18	12.59	100.00	0.00
0.141	1.74	1.05	1.41	99.79	0.59	14.13	100.00	0.00
0.159	3.44	1.69	1.59	99.98	0.20	15.85	100.00	0.00
0.178	5.89	2.46	1.78	100.00	0.02	17.78	100.00	0.00
0.199	9.22	3.33	2.00	100.00	0.00	19.95	100.00	0.00
0.224	13.48	4.26	2.24	100.00	0.00	22.39	100.00	0.00
0.251	18.66	5.18	2.51	100.00	0.00	25.12	100.00	0.00
0.282	24.74	6.08	2.82	100.00	0.00	28.18	100.00	0.00
0.316	31.66	6.91	3.16	100.00	0.00	31.62	100.00	0.00
0.355	39.23	7.57	3.55	100.00	0.00	35.48	100.00	0.00
0.398	47.23	8.00	3.98	100.00	0.00	39.81	100.00	0.00
0.447	55.40	8.17	4.47	100.00	0.00	44.67	100.00	0.00
0.501	63.44	8.03	5.01	100.00	0.00	50.12	100.00	0.00
0.562	71.04	7.60	5.62	100.00	0.00	56.23	100.00	0.00
0.631	77.98	6.94	6.31	100.00	0.00	63.10	100.00	0.00
0.708	84.03	6.05	7.08	100.00	0.00	70.79	100.00	0.00
0.794	89.08	5.06	7.94	100.00	0.00	79.43	100.00	0.00
0.891	93.08	4.00	8.91	100.00	0.00	89.13	100.00	0.00
1.00	96.03	2.95	10.00	100.00	0.00	100.00	100.00	0.00

Figure 20 - Homemade suspension particle size distribution

3.3 Spray process

The process parameters used to spray the samples in this work are described in Table 2. The plasma gun used in the experiments was the 3MB (Oerlikon Metco, USA). This gun has a water-cooled electrode, the anode, and a tungsten cathode, generating an arc current of 600 A, with plasma forming gases: argon, as the primary gas, and helium, as the secondary gas. The power used to spray the coatings was 24 kW and the velocity of the torch spray was 1 m/s.

Table 2 – Plasma spray parameters

Plasma gun:	3MB (Oerlikon Metco)
Plasma gases:	Argon – 25 Lpm Helium – 25 Lpm
Current:	600 A
Voltage:	40 V
Power:	24 kW
Standoff distance:	40 mm
Torch spray velocity:	1 m/s

The suspension injection was radial, external to the plasma gun with the injector oriented 15° towards the gun exit as shown in Figure 21. The standoff distance was kept constant for all the experiments as 40 mm in front of the substrates.

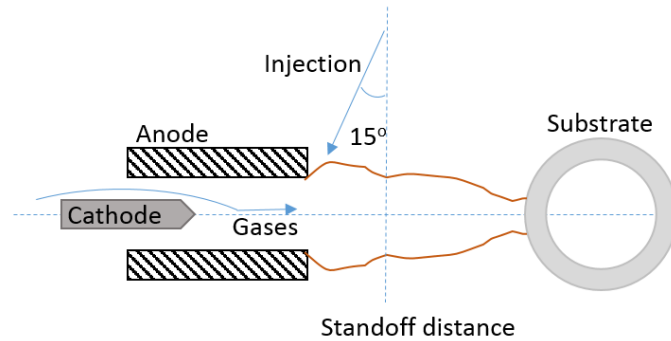


Figure 21 - Schematic of the suspension injection into the plasma get

This work was performed in two parts. First, a preliminary study was performed spraying three different standoff distances (30, 40 and 50 mm) and two shapes (flat and cylinder). After the preliminary study, it was decided to keep only 40 mm as standoff distance and add one more shape (rod sample), in order to focus on the substrate shape and roughness. The width of the coating footprint measured in the preliminary study was around 1 cm. In order to have a curved substrate smaller than the footprint of the coatings, the rod samples were added.

The spraying strategy used in this work was to spray one straight line horizontally in front of the substrate. The torch was positioned in a way that its axis was scanned over a horizontal line on the center of substrate (Figure 21). The torch was then moved only horizontally, completing multiple passages (scans) in front of the substrate. This strategy was chosen in order to make it

simple to see the effect of the shape in one single bead. Moreover, spraying one straight line would be useful to validate the numerical results from Pourang et al. [37] and also for further numerical modeling comparison.

For this study, two series of samples were sprayed. In the first batch, nine samples (three shapes and three roughness) were sprayed separately. Fifty scans in front of the substrates built the coatings. After analyzing the results, a second batch of samples was sprayed with double number of scans (one hundred scans), in order to build thicker coatings and observe a further development of the microstructures.

In the second batch of samples they were sprayed by shape. The three different roughness were fixed side by side in the sample holder for each shape, and consequently, sprayed at the same time, with the same exact conditions. These samples were pre-heated to temperatures close to 100 °C, monitored by an Infrared Camera (FLIR Systems, USA), before the suspension started to be injected. The samples were sprayed with one hundred scans of the torch in front of them.

3.4 Design of experiments

In total, 18 types of samples were sprayed, combining the shapes, surface treatments and number of scans. The samples were labeled with three characters:

- The first character stands for the batch: “4” means the first series of samples with 50 scans and 4 cm of standoff distance, and “T” stands for thicker coatings, the ones sprayed with 100 scans at 4 cm of standoff distance.
- Second character is for surface roughness: “P” is for polished substrates, “F” means fine grit blasting and “C” is for coarse grit blasting.
- The third letter: “F” means flat samples, “C” is for cylinder and “R” for rod samples.

Table 3 shows all the samples and parameters of sprayed samples:

Table 3 – Design of experiments of samples sprayed

Sample	# of passes	Shape	Roughness
4PF	50	Flat	Polished
4FF	50	Flat	Fine
4CF	50	Flat	Coarse
4PC	50	Cylinder	Polished
4FC	50	Cylinder	Fine
4CC	50	Cylinder	Coarse
4PR	50	Rod	Polished
4FR	50	Rod	Fine
4CR	50	Rod	Coarse
TPF	100	Flat	Polished
TFF	100	Flat	Fine
TCF	100	Flat	Coarse
TPC	100	Cylinder	Polished
TFC	100	Cylinder	Fine
TCC	100	Cylinder	Coarse
TPR	100	Rod	Polished
TFR	100	Rod	Fine
TCR	100	Rod	Coarse

After sprayed, the samples were characterized and observed under the SEM.

3.5 Coating characterization

Some measurements were taken from the samples before, during and after spraying. Samples were weighed before and after spraying and also the roughness was measured with a Profilometer (Mitutoyo, Japan) in the center of the substrate before and after spraying. The substrate temperature was monitored during spraying with an Infrared Camera (FLIR Systems, USA). In addition, microstructure observation was performed after spraying. All samples were sectioned, cold-mounted, grinded and polished.

The cutting, mounting and polishing instruments and consumables were from Struers (Denmark). The first metallographic process was the sectioning. The samples were cut in a high

precision cut-off machine, Secotom 15, in order to analyze the cross-section of the coatings. The cut-off wheel used was 50A20 (Aluminum Oxide), which was selected according to the hardness of the material. The cutting program was different for the different shapes of samples. Overall, the rotation speed used was 2500 rpm and the feed speed of the moveable table between 0.02 and 0.05 mm/s.

After sectioned, the samples were mounted into room-temperature curing resin. The sections of samples were placed into rubber molds and the mix of epoxy resin system were added to it. The epoxy system used was EpoFix, a transparent epoxy resin and hardener, in the volume ratio of 15 mL of resin to 2 mL of hardener. In order to help forming a homogeneous impregnation, the molds containing the samples and resin were put under vacuum during 15 minutes at a pressure of 12 kPa using the CitoVac. After the vacuum impregnation process was finished, the resins stayed curing for about 10 hours.

Once the resin is cured, the mounted samples were grinded and polished in the Tegramin-25 polishing system to obtain a polished surface appropriate for metallurgical observation under low and high magnifications. The process started with fixing the mounted samples in the sample holder. After that, the wet grinding of the samples was done with 3 different silicon carbide grinding papers, grit 320, 500 and 800. Following grinding, other 4 steps of polishing were done.

First step of polishing, the MD-Plan polishing cloth, which is made of polyester was used as a pre-polishing along with a water based diamond suspension lubricant DiaDuo-2, 9 μm . Second polishing cloth used was MD-Dac, a satin woven acetate with the water based diamond suspension lubricant DiaDuo-2, 3 μm . After that, the MD-Nap polishing cloth was used with the water based diamond suspension lubricant DiaDuo-2, 1 μm . In the last step of the process, MD-Chem polishing cloth was used for final polish with a non-drying colloidal silica suspension, OP-S NonDry.

Once metallographic preparation was done, the samples were observed under the SEM. The device used was a Hitachi (Japan), S-3400N. The mapping of the samples cross-sections was done with secondary electron (SE) detector. Several pictures were taken from the coatings observed,

in order to perform image analysis. The mounted samples received a thin Au coating through gold sputtering, in order to decrease charging effect in the SEM.

The pictures recorded were taken with different magnifications. Most of the pictures were taken with magnification of x2k, x1k or x500. The image analyses of all the samples sprayed will be presented in chapter 4. Further analysis and the results of this work are described in the next chapter.

4. Results and Discussion

As stated before, the aim of this work was to investigate the effects of the substrate curvature and roughness on the coating microstructure. This chapter will show the results of the work, after spraying the coatings and analyzing their microstructure under the SEM.

4.1 Results

Images were recorded from SEM observation and analyzed with software ImageJ in a more detailed way. Measure of thickness of the coatings and width of columns were performed. For each point of interest in the coating, the thickness was measured in a systematic way: every 30 μm , one measurement was recorded. The column measurement was done only where columns were observed. The width of the columns was measured and recorded. A column was considered as such if its width is smaller than the thickness in that point and its length is at least one half of the thickness.

Shadow effect is also present in most of the coatings. Shadow effect can be described as a local thickness variation, where it is possible to see a bump along with a depression right beside. All the images are presented in their locations along the axis of the samples. The position 0 is the center of the sample, it is the location where the torch was aligned to scan the samples horizontally. The negative side of the samples means the bottom side of the sample during spray, in other words, below the torch axis. Finally, the positive side of the samples is the top side of the sample during spray, above the torch, and in the same side as the radial suspension injection. Each position is represented by its distance (mm) along the surface of the sample measured from its center. The information extracted from the images is presented in this section.

4.1.1 Thin flat samples

The first samples analyzed were the flat samples. This kind of coupons are very often used in research. Figure 22 shows the top and cross-section views for the coarse flat thin sample (4CF). The top view represents the surface of the coating, where the roughness was measured after spraying. In 4CF it is possible to observe that the highest thickness was in the center of deposition. As it gets farther from the center of the deposition, the thickness decreases and the porosity

increases. Additionally, it is possible to see some shadow effect as it gets farther from the center of deposition, indicated by the arrow in Figure 22.

However, in the fine flat sample (4FF) (Figure 23) the shadow effect is less prominent. On the other hand, the thickest part of the coating in 4FF is also observed to be in the center of the deposition, and the thickness decreases as it gets closer to the end of the footprint.

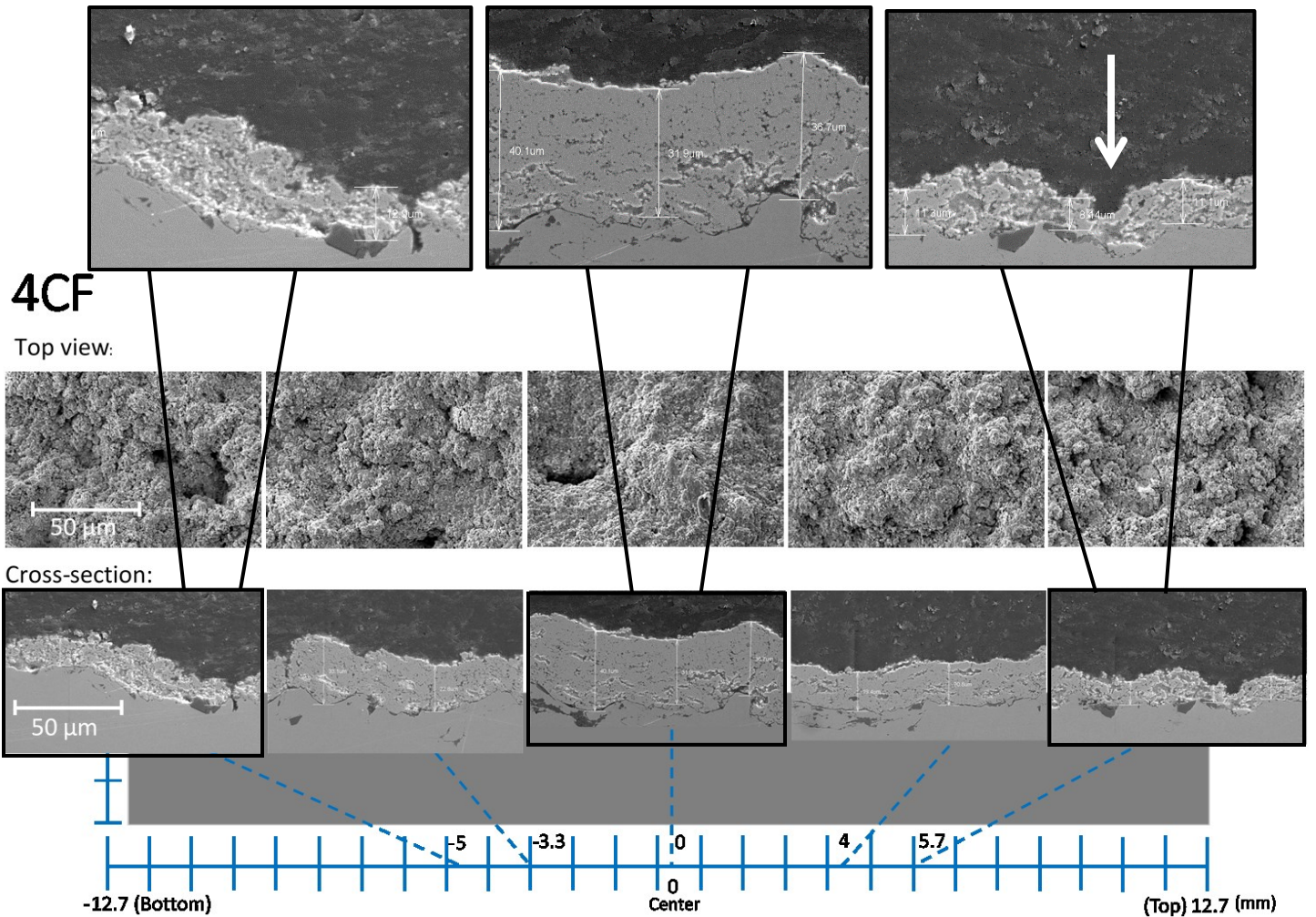


Figure 22 - Thin Coarse Flat (4CF) cross-section and top view SEM images

When the surface of the sample was polished (sample 4PF in Figure 24), it is evident that delamination of the coating has occurred, as indicated by the arrow. It is not possible to identify where the highest thickness was located, since the coating did not stick to the substrate. Columns are not present in this coating and the shadow effect is very small as well.

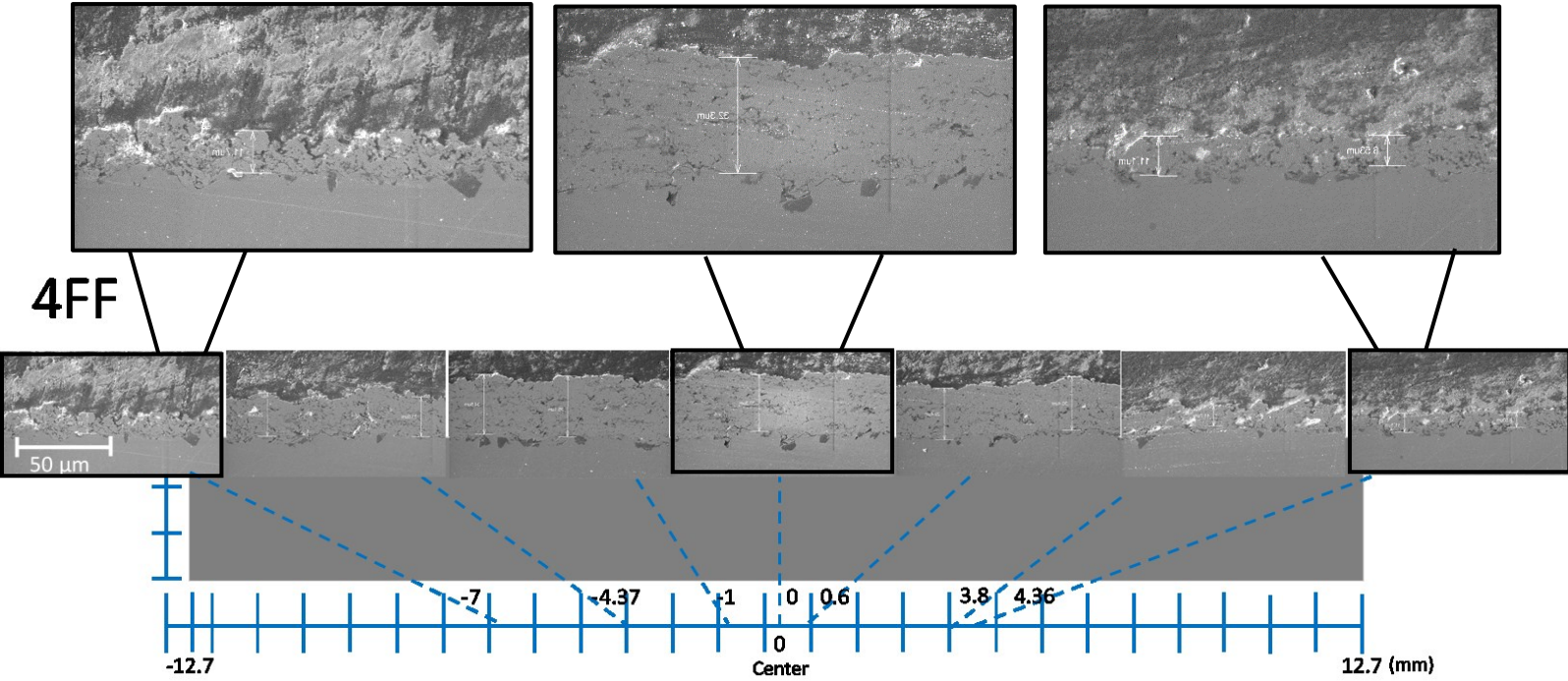


Figure 23 - Thin Fine Flat (4FF) cross-section SEM images

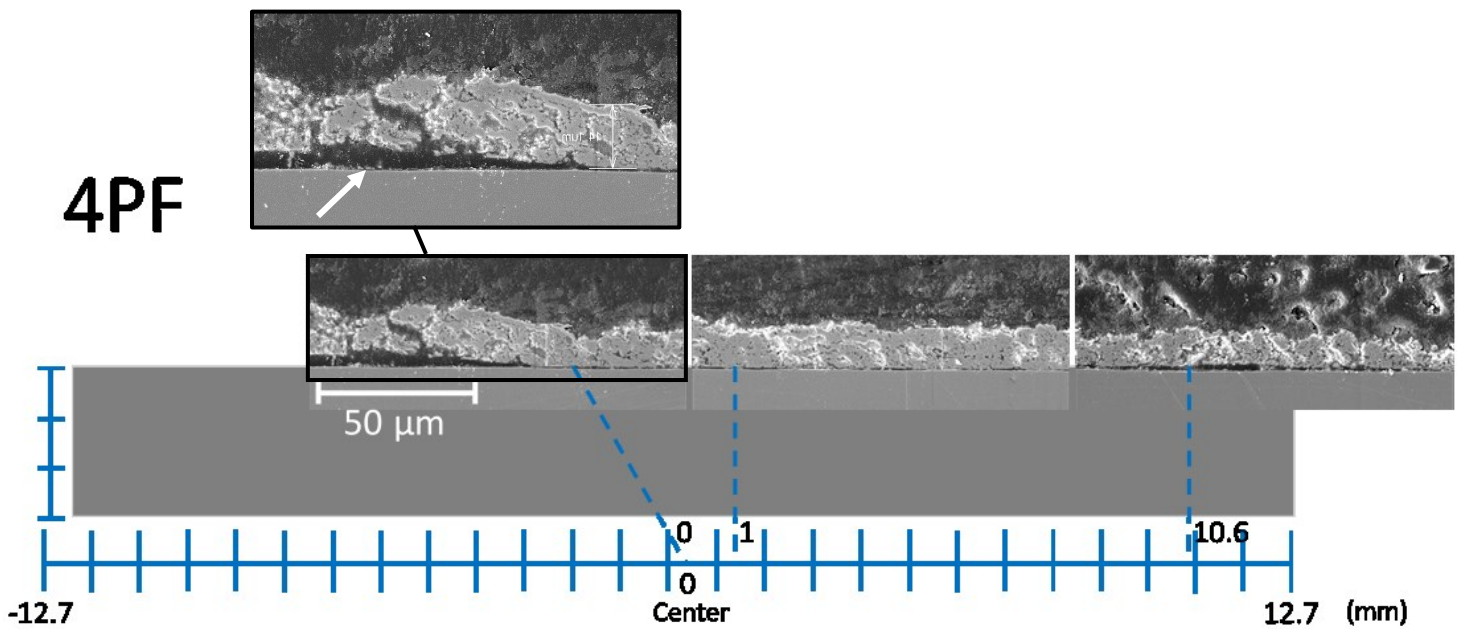


Figure 24 - Thin Polished Flat (4PF) cross-section SEM images

In all the thin flat samples sprayed, columnar structure was not observed. There was an increase in the shadowing effect as the roughness was increased. Moreover, when the surface was too smooth the coating did not adhere to the substrate.

The thickness measured for the thin flat samples is shown in Table 4.

Table 4 – Thickness of Thin Flat samples in different positions

Position	THICKNESS (μm)					
	4PF		4FF		4CF	
	Mean	Std dev.	Mean	Std dev.	Mean	Std dev.
-4	14.7	3.43	23.2	2.08	19.4	8.14
-3	14.5	1.17	31.9	1.1	25	4.11
0			33.5	1.19	37.	5.45
4			11.5	3.3	20.5	1.68
5.7	11.1	1.95	7.7	1.11	13.9	2.13

The graph in Figure 25 a) shows the thickness of the three thin flat samples in the same positions along the axis. In 4PF, as previously showed in the SEM images, delamination occurred in the center of the substrate. For 4FF and 4CF, it is possible to see that thickness is bigger in the center towards the bottom of the substrate.

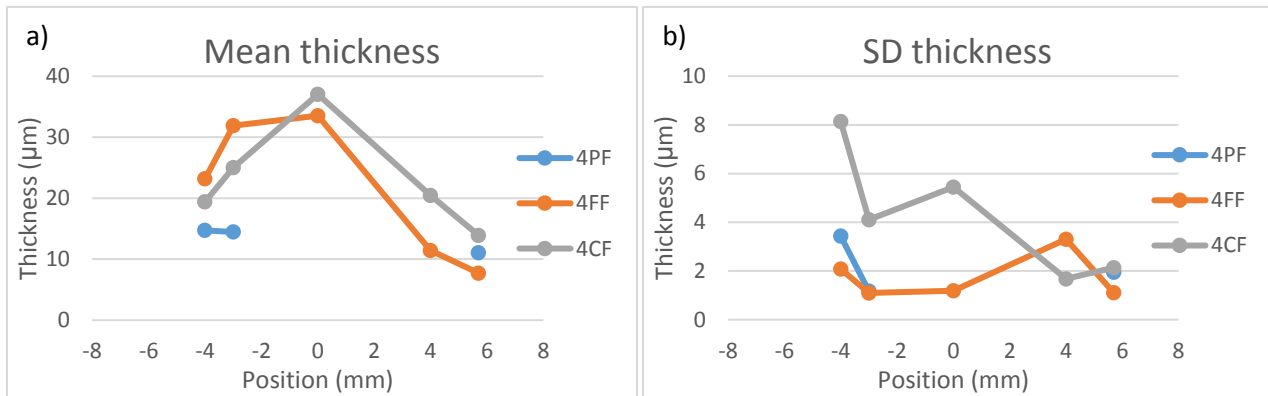


Figure 25 - a) Thickness measured for Thin Flat samples, and b) variation of thickness for Thin Flat samples

Figure 25 b) shows the standard deviation of the thickness measured in each position. It is possible to see that due to the shadow effect in the bottom side, as already pointed out in the SEM images, there are some large variation of the thickness, thus a higher standard deviation. Additionally, in the center of 4FF it is observed a low variation of the coating thickness. This can be explained by the absence of shadow effect due to its smooth surface. However, on the top side of 4FF, where some shadow effect starts to appear, the variation of the thickness is also higher.

Substrate roughness was measured before spraying, and after spraying the roughness of the coating was measured in different locations. Figure 26 shows the roughness measured before and after spraying for the thin flat samples.



Figure 26 - Roughness measured for Thin Flat samples

4.1.2 Thin cylinder samples

Cylinder samples started to show different structures. In the thin coarse cylinder sample (4CC) (Figure 27), it is possible to see more shadow effect due to the roughness and the geometry of the sample. Additionally, the cylinder samples presented some column-like structures, as shown in Figure 28 and Figure 29, thin fine and thin polished cylinder samples, respectively. The orientation of the columns in 4FC is not very clear, but it seems to be perpendicular to the surface of the substrate. The fine cylinder sample also showed a few vertical cracks.

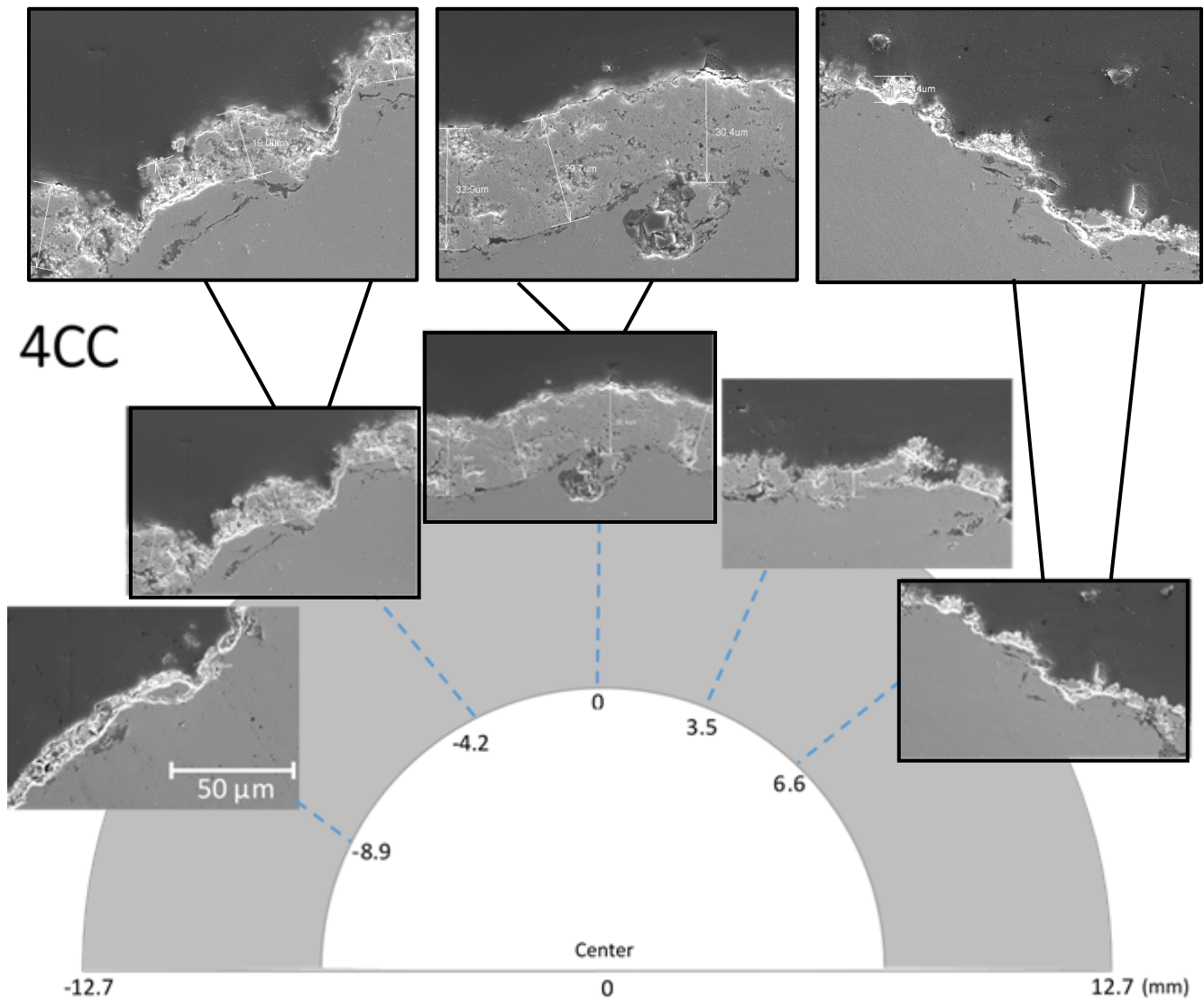


Figure 27 - Thin Coarse Cylinder (4CC) cross-section SEM images

The thin polished sample presented well-defined tiny columns on the top side of the substrate. The polished cylinder sample had delamination, as it also happened to the flat polished sample. Delamination can be seen in Figure 29, where the coating is detached from the sample in the center (indicated by the arrow) and it is also missing in other parts of the surface. The columns observed on the bottom side of this sample appear to have an orientation perpendicular to the substrate. On the other hand, the columns present on 4PC top side show an orientation parallel to the torch axis.

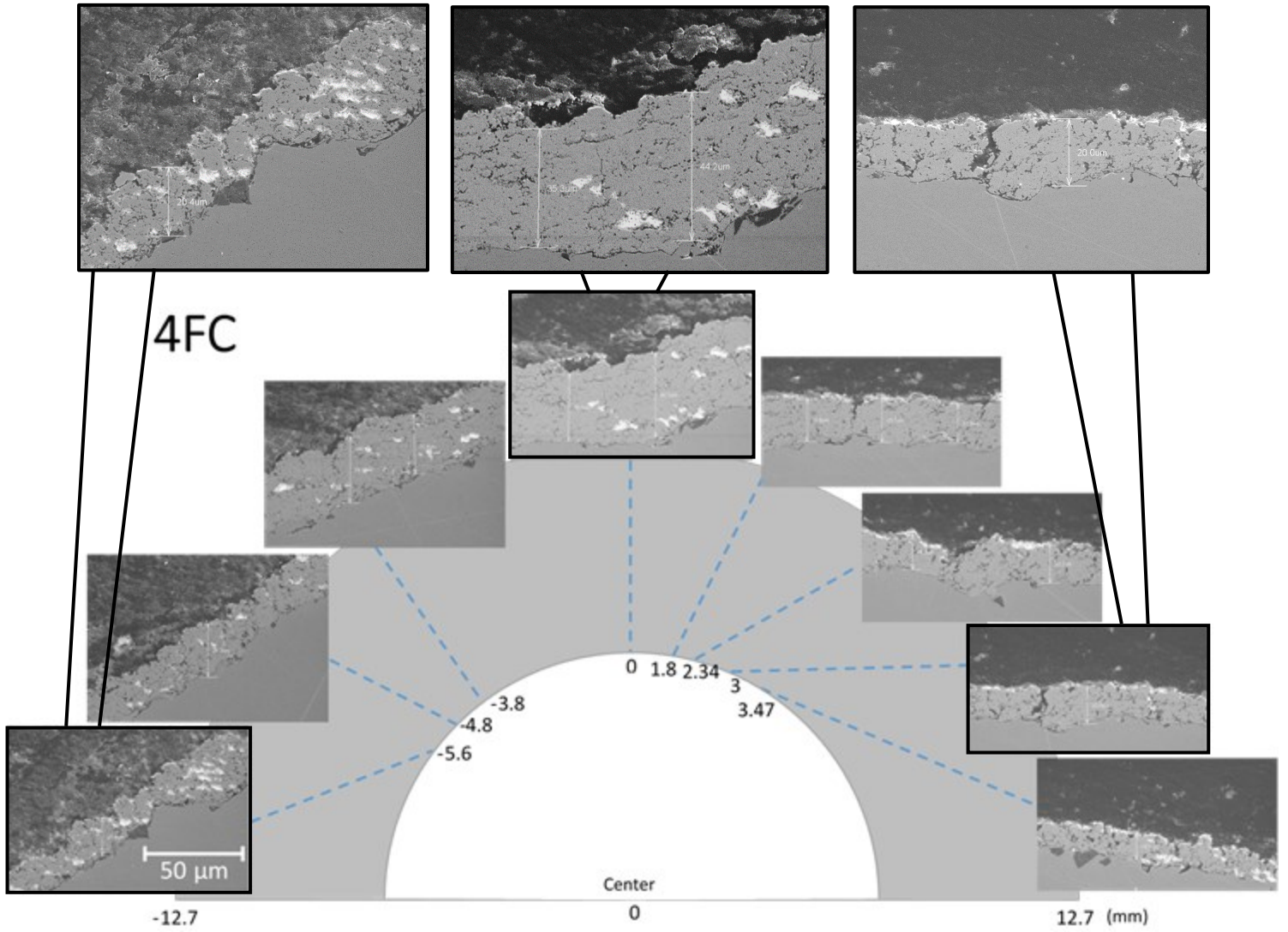


Figure 28 - Thin Fine Cylinder (4FC) cross-section SEM images

The thin cylinder samples also formed the thicker part of the coating in the center of the substrate, towards the bottom side as Table 5 shows. In Figure 30 a), this is possible to see in 4FC and 4CC. 4PC had delamination as the SEM images showed. Figure 30 b) also shows the large variation in the thickness measured in 4CC due to the shadow effect. The columns and vertical cracks present in 4FC also made the thickness variation increase.

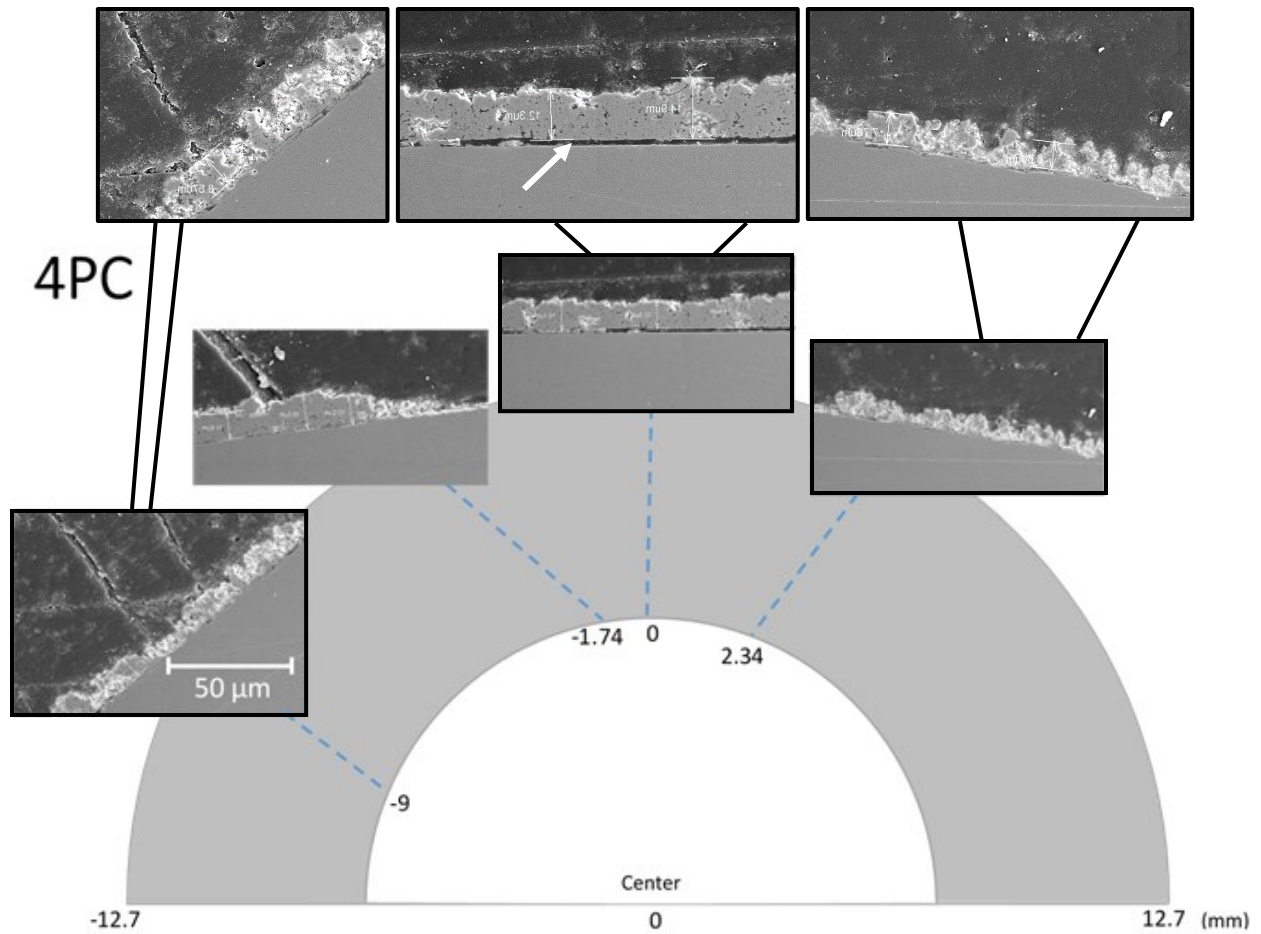


Figure 29 - Thin Polished Cylinder (4PC) cross-section SEM images

Table 5 – Thickness of Thin Cylinder samples in different positions

THICKNESS						
Position	4PC		4FC		4CC	
	Mean	St dev	Mean	St dev	Mean	St dev
-9	8.5	2.95	22.5	4.19	7.9	2.65
-3.8			34.7	1.92	18.7	8.19
-1.7	13.6	1.29	43.8	3.08	28.3	1.88
0	13.2	1.08	44.1	4.42	28.3	3.75
2.3	8.2	0.16	21.3	2.87	14.9	4.52
3.4			13.1	2.91	7.5	4.58

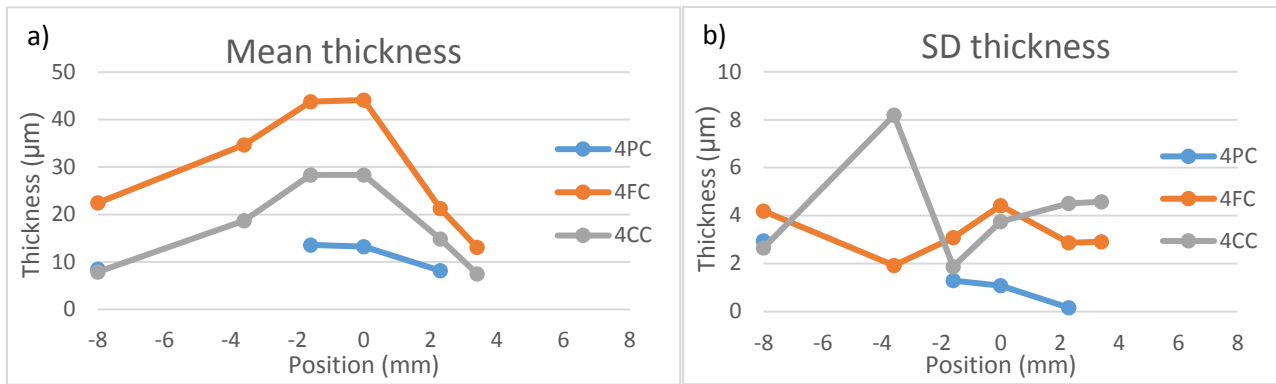


Figure 30 - a) Thickness measured Thin Cylinder samples, and b) variation of thickness for Thin Cylinder samples

For roughness measurements, Figure 31 a) shows that there is not very big variation in the roughness measured before and after spraying. The end of the footprints for 4CC and 4FC show more columns and shadow effect, consequently the roughness has also increased in those points.

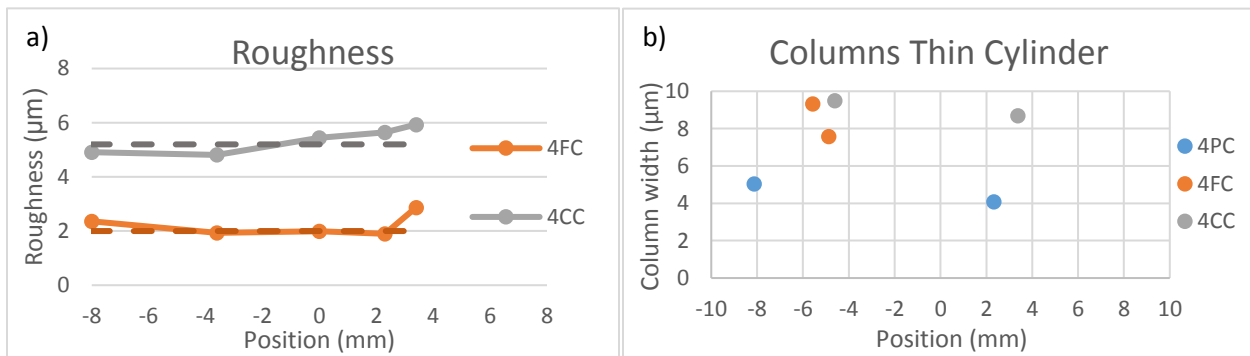


Figure 31 - a) Roughness measured for Thin Cylinder samples, and b) columns width measured for Thin Cylinder samples

Figure 31 b) shows the width of the columns measured. As previously seen in the SEM images, 4PC had tiny columns while 4FC and 4CC presented some wider columns.

4.1.3 Thin rod samples

The thin rod samples observed presented the same structure of fine columns, possibly in more quantity, as it can be seen in Figure 32 coarse rod sample (4CR). Clearly, the top side of the sample has a denser coating and there are more columns in the bottom side of the substrate than the top.

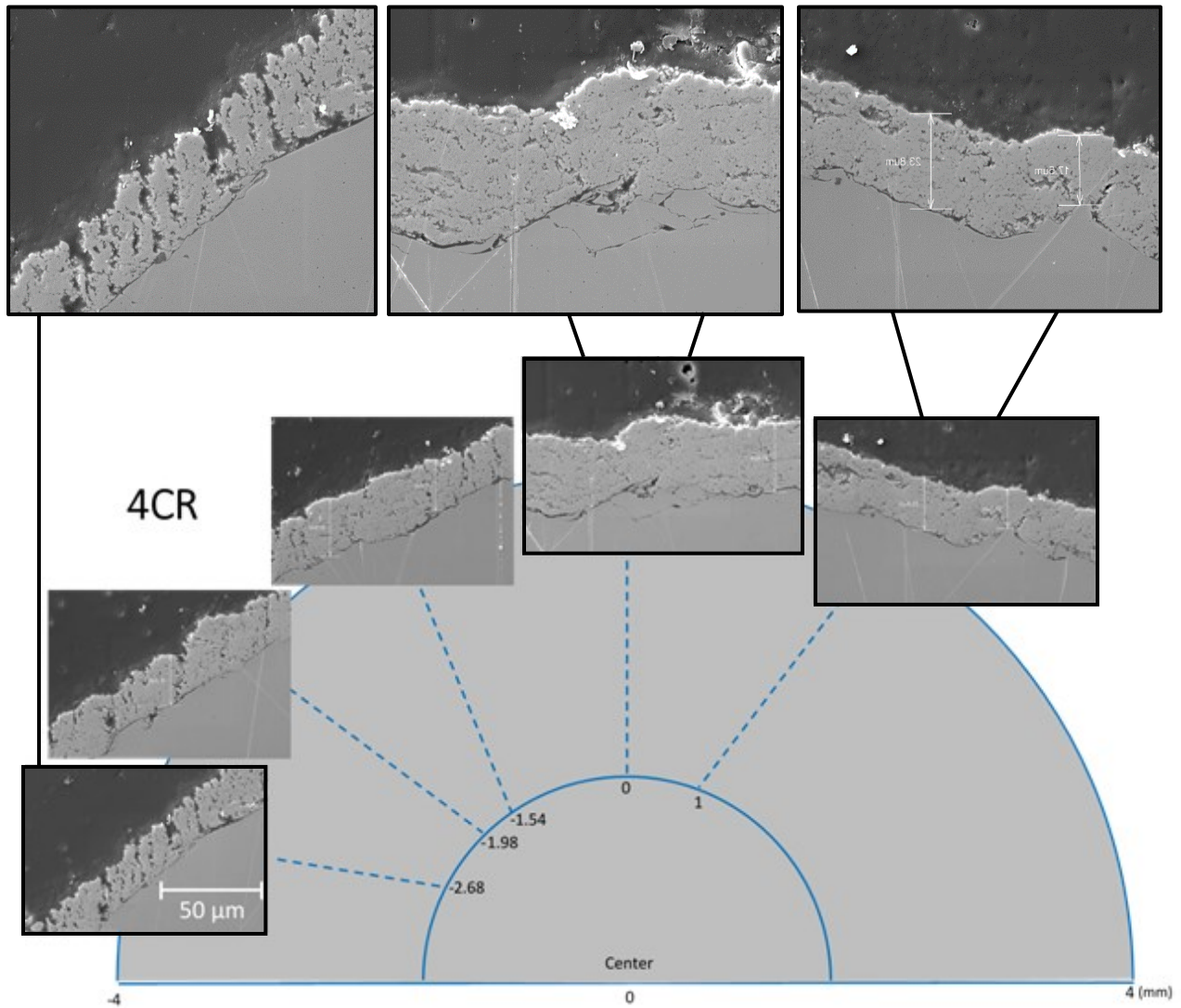


Figure 32 - Thin Coarse Rod (4CR) cross-section SEM images

The thin fine rod sample, however, presented a slightly different structure when compared to the other fine samples. On the bottom side, 4FR presented a denser coating, where it is possible to see some layers instead of columns (Figure 33). On the other hand, some columns can be seen on the top side, closer to the end of the footprint. For the polished rod sample (4PR), the columns are very well defined on the bottom side of the sample, and delamination is also present in the center of the substrate, as shown in Figure 34.

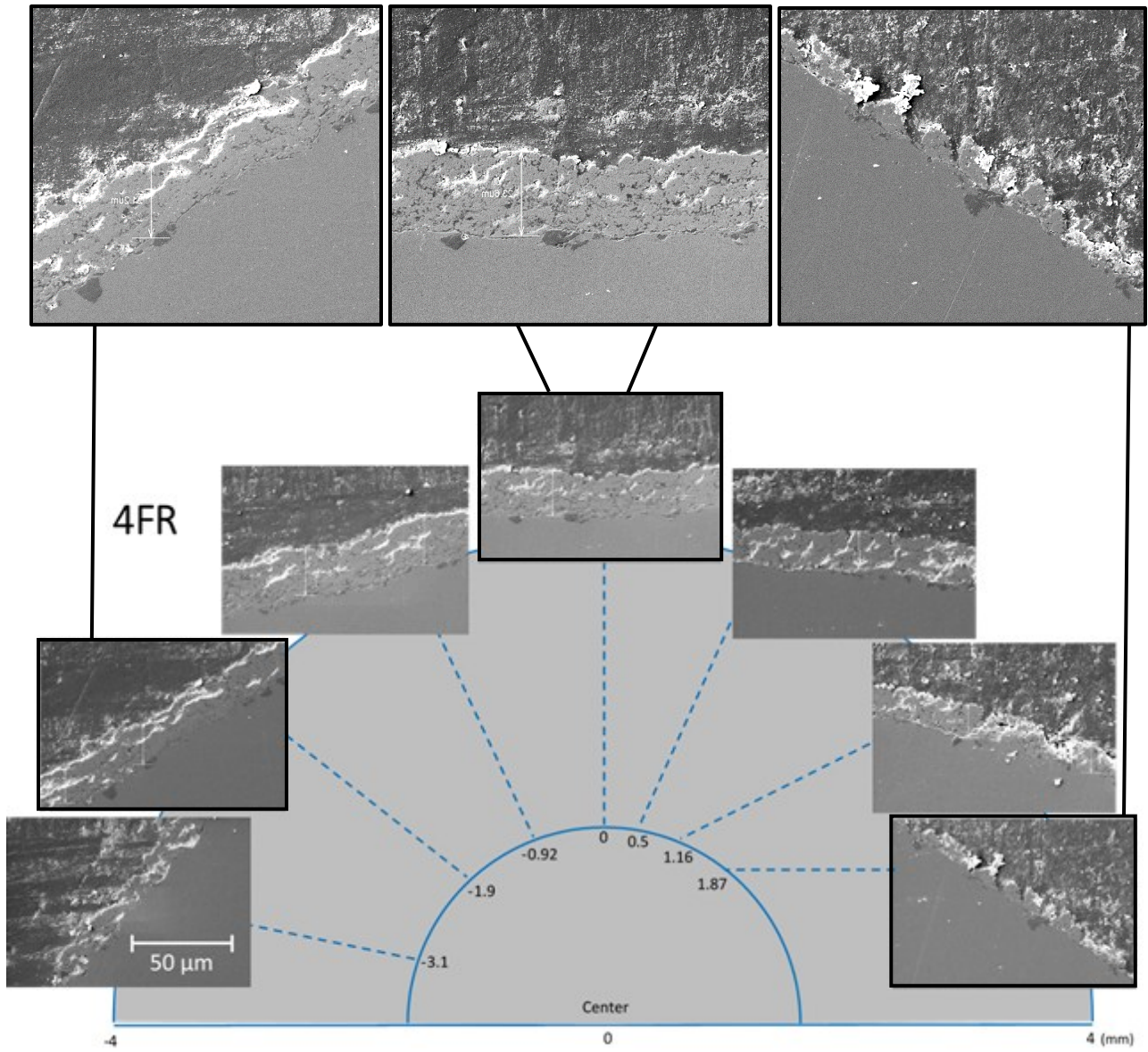


Figure 33 - Thin Fine Rod (4FR) cross-section SEM images

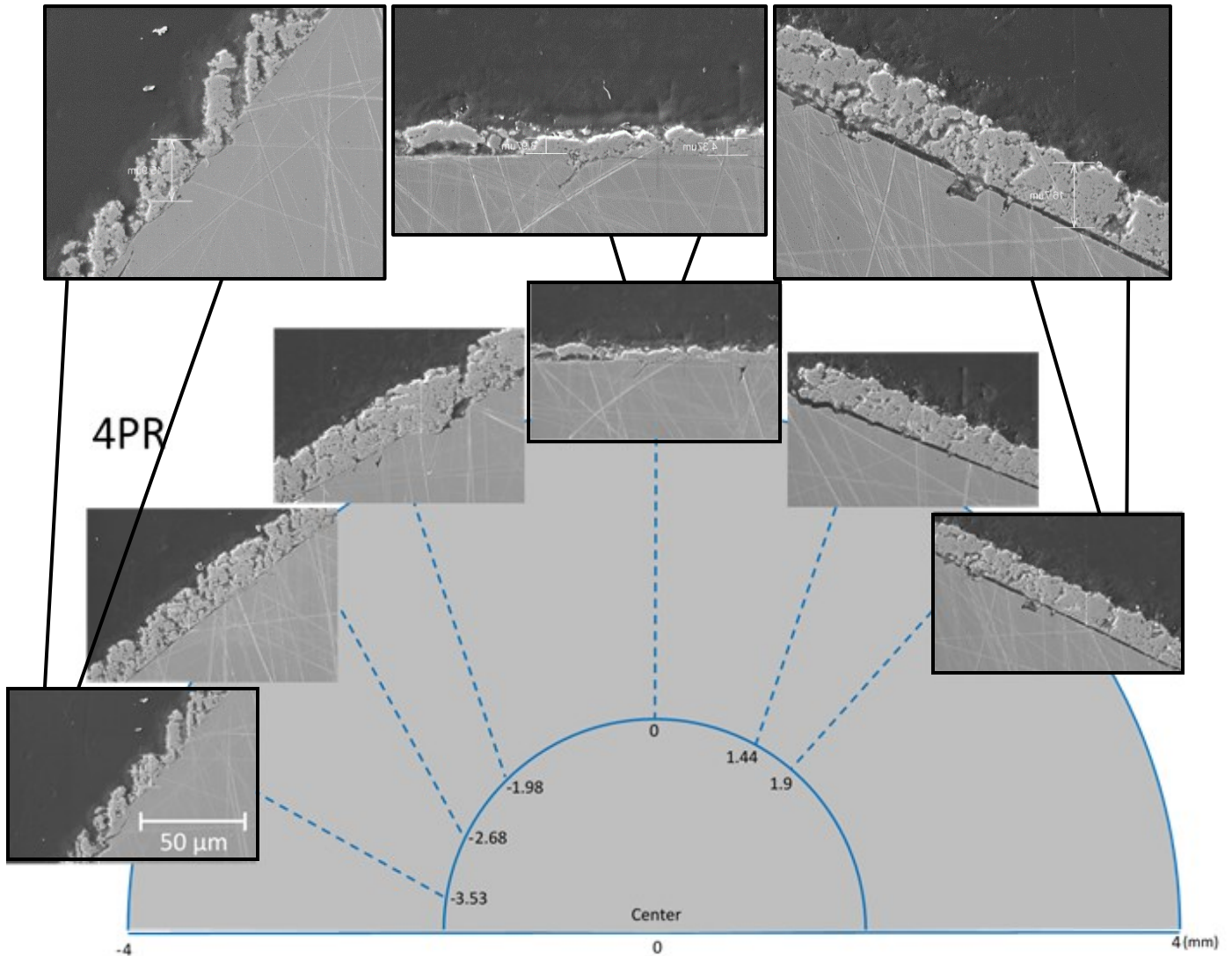


Figure 34 - Thin Polished Rod (4PR) cross-section SEM images

Thin rod samples had delamination only in the polished surface. Table 6 shows the thickness measured for all the thin rod samples. As Figure 35 a) shows, the thicker part of the coatings 4FR and 4CR are again in the center and bottom part of the coatings. It is possible that the coating in 4PR follows the same pattern, however, it cannot be affirmed at this point because of coating delamination. Due to the high amount of columns on the bottom side of the samples, in 4PR and 4CR, as Figure 35 b) shows, there is some variation on the thickness measured. 4FR, on the other hand, has a higher variation of thickness on the top side, where columns are identified.

Table 6 – Thickness of Thin Rod samples in different positions

THICKNESS						
Position	4PR		4FR		4CR	
	Mean	St dev	Mean	St dev	Mean	St dev
-3.2	17.5	0.13	17.1	0.6	27.6	1.8
-2.6	22.8	1.33	20.1	1.11	26.1	0.34
-1.8	24.9	3.79	25.2	1.03	27.7	3.41
-0.8	26.9	0.92	26.3	1.8	29.2	2.54
0			21.8	0.36	31.7	0.36
1			14.8	2.76	24.6	2.91
1.4	18.3	0.64	16.7	3.39	23.4	1.84
1.8	16.3	1.28	8.4	0.71	20.2	3.54

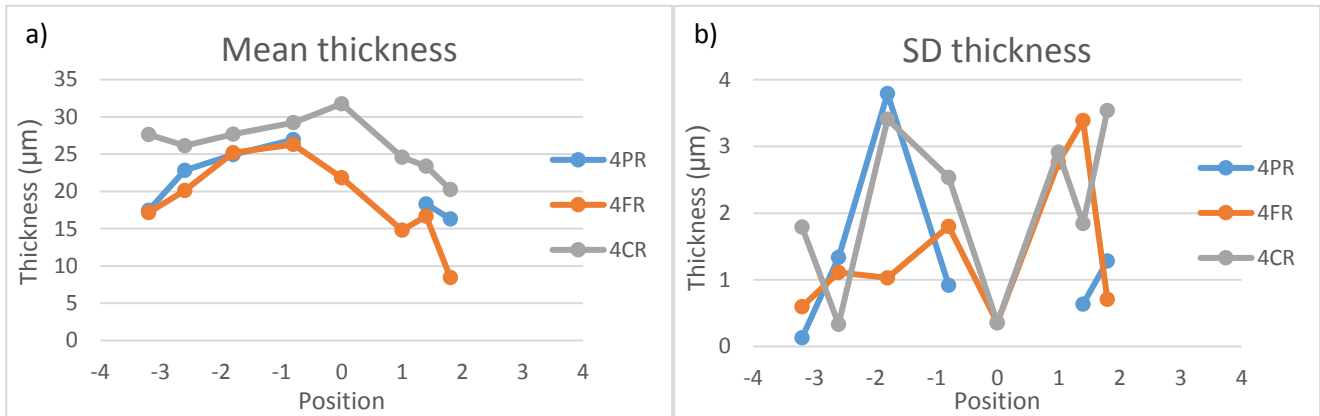


Figure 35 - a) Thickness measured for Thin Rod samples, and b) variation of thickness for Thin Rod samples

The roughness measured before and after spraying showed in Figure 36 a), brings a bigger difference in the roughness on the bottom side of the coatings. This might have happened due to the difficulties of grit-blasting a curved substrate and achieve the same roughness in the whole surface. It seems that the surface before spraying was smoother on 4CR and coarser in 4FR, both on the bottom side.

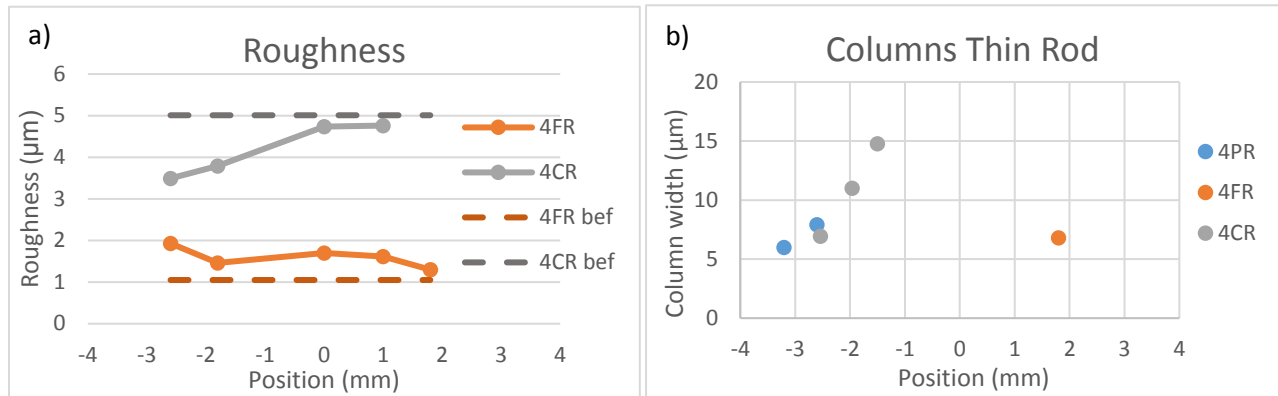


Figure 36 - a) Roughness measured for Thin Rod samples, and b) columns width measured for Thin Rod samples

The columns measurement for the thin rod samples shows that for 4PR and 4CR, the column width decreases as it gets closer to the end of the footprint (Figure 36 b)). As seen in the SEM images, 4FR presented a different structure and columns only on the top side.

4.1.4 Thick flat samples

For the second batch of samples, they were sprayed with the same exact conditions to minimize uncontrollable parameters. For each shape, the three samples with different roughness were placed side by side in the sample holder. This means that they had the same number of passes during pre-heating and spraying, the same spray conditions and same suspension composition. All the samples for the second batch were also sprayed in the same day, thus, the same batch of homemade suspension was used to spray all the samples.

The thick samples were sprayed with a double number of passes: 100 passes. These samples were also pre-heated at about 100°C before starting spraying the suspension. As it can be seen in Figure 37, Figure 38 and Figure 39, samples TCF, TFF and TPF respectively, the highest thickness happened in the center of samples, towards the bottom side. No delamination is present in any roughness (coarse, fine or polished) for flat samples.

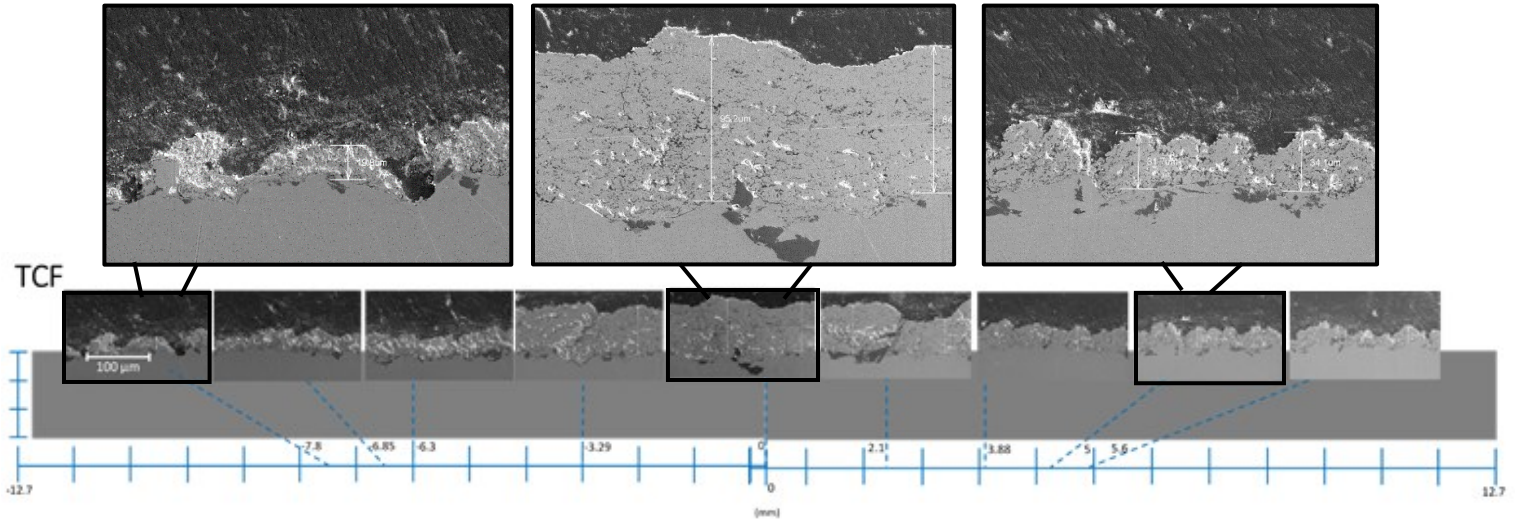


Figure 37 - Thick Coarse Flat (TCF) cross-section SEM images

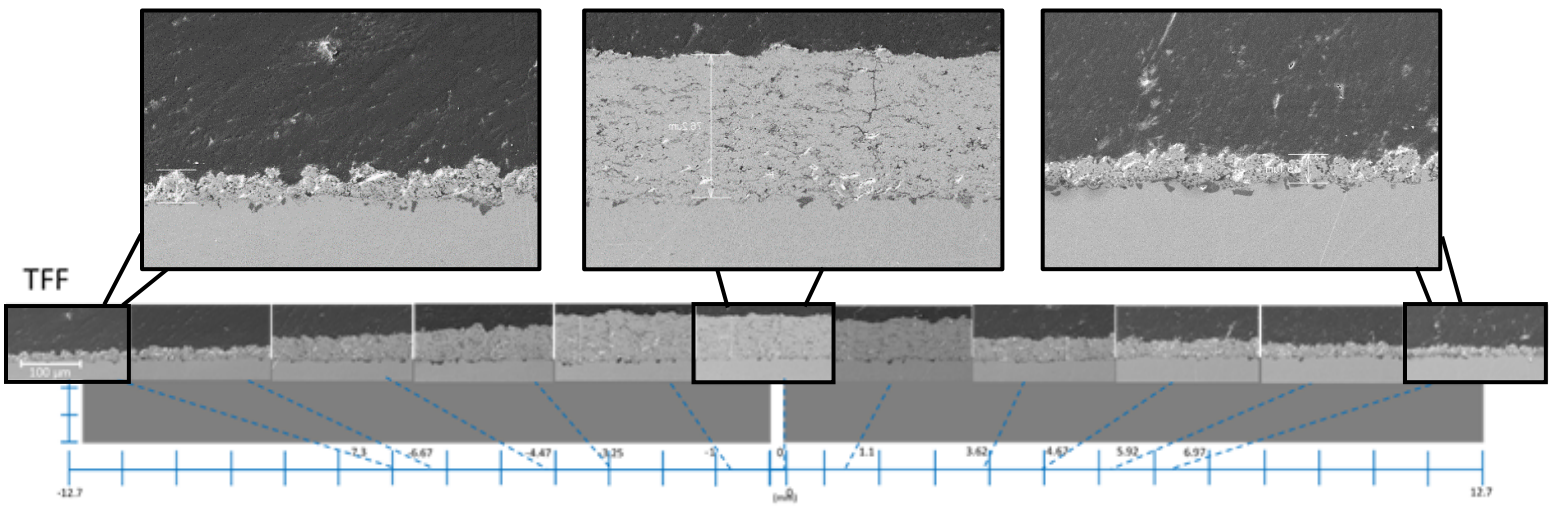


Figure 38 - Thick Fine Flat (TFF) cross-section SEM images

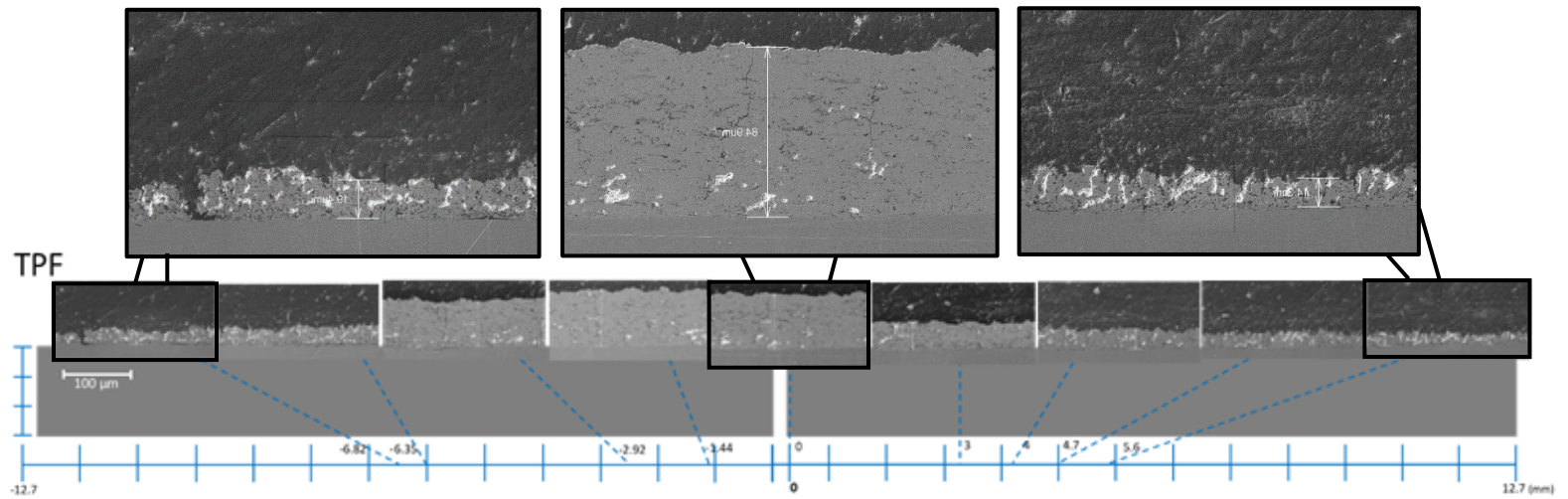


Figure 39 - Thick Polished Flat (TPF) cross-section SEM images

It is possible to see strong shadowing effect in the coarse flat sample, and a light shadow effect towards the end of the coating footprint in the fine and polished flat samples. Some tiny columns can also be seen in the end of the coating footprints.

The thick flat samples revealed similar results to thin flat samples. Table 7 shows the thickness measured for the three roughness:

Table 7 – Thickness of Thick Flat samples in different positions

THICKNESS						
Position	TPF		TFF		TCF	
	Mean	Std dev.	Mean	Std dev.	Mean	Std dev.
-6.8	22.3	3.33	18.9	1.75	27.4	4.72
-3	71.3	3.35	57.6	3.74	81.4	8.26
0	84	1.27	76.2	2.27	90.9	5.91
4	26.7	3.51	40.1	2.14	35.9	7.8
4.7	24.1	2.4	29.6	4.9	31.9	5.66
5.6	18.3	2.4	22.8	3.9	22.8	7.73

Likewise the thin flat samples, all the thick flat samples had the thicker part of the coating in the center, towards the bottom side of the substrate (Figure 40 a)). Moreover, due to the coarse surface of TCF and shadow effect present in the coating, the variation of the thickness in each position is higher. The light shadow effect in the end of the coating footprint in addition to the small columns for TPF and TFF also made the variation increase on that positions, as shown in Figure 40 b).

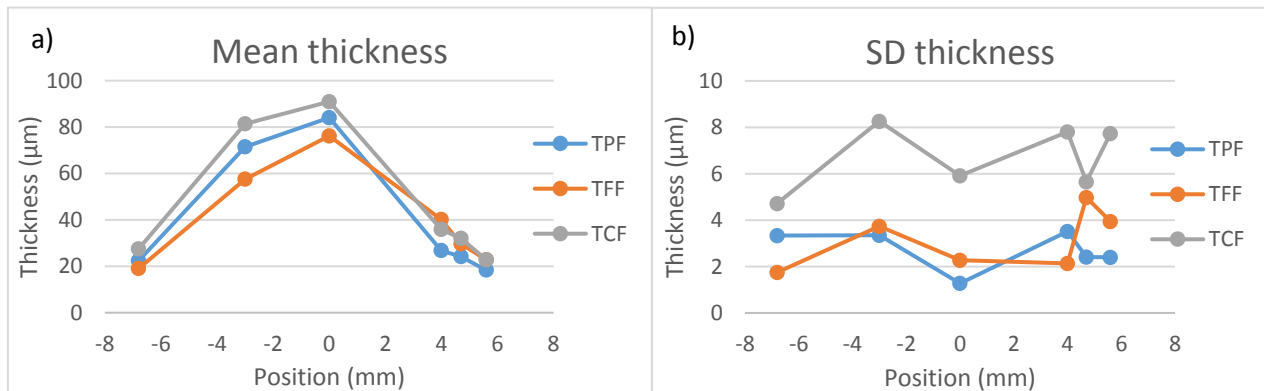


Figure 40 - a) Thickness measured for Thick Flat samples, and b) variation of thickness for Thick Flat samples

The roughness measured for the thick flat samples is shown in Figure 41 a). Roughness changes are bigger in the end of coating footprint due to the shadow effect and columns. In the

center of the substrate, the roughness after spray is very similar to the roughness before spray because the coating follows the substrate roughness without columns or shadow effect.

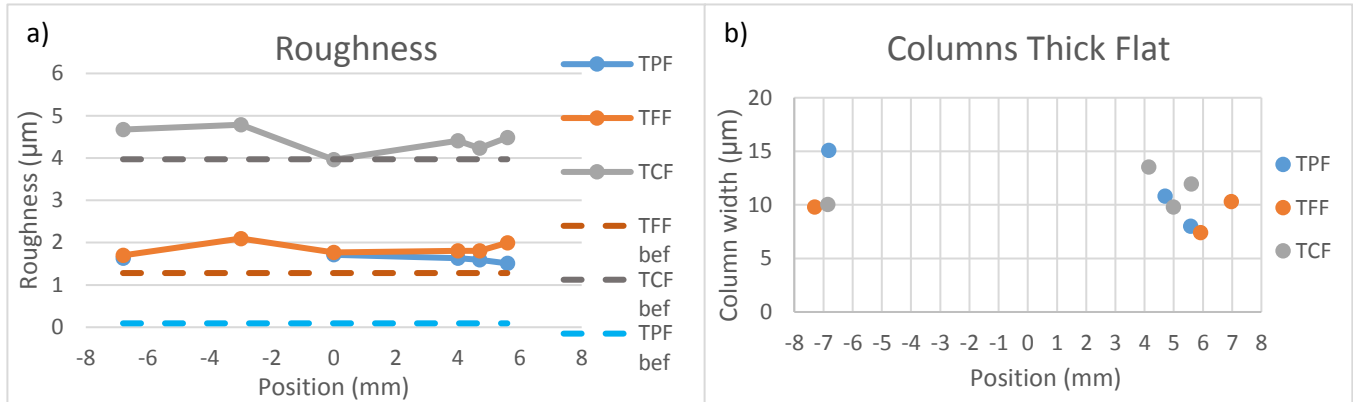


Figure 41 - a) Roughness measured for Thick Flat samples, and b) columns width measured for Thick Flat samples

In Figure 41 b) the columns width measurements are presented. In all the thick flat samples columns were observed on both top and bottom sides.

4.1.5 Thick cylinder samples

In the cylinder samples, delamination occurred independently of the substrate roughness. As shown in Figure 42, thick coarse cylinder (TCC), columns are present mostly in the bottom side of the substrate, close to the end of the coating footprint. Also, it is possible to see the shadow effect within the coating, in the top and bottom sides. The same also happened for the fine cylinder sample (TFC), being the shadow effect less strong, probably due to the smoother surface (Figure 43).

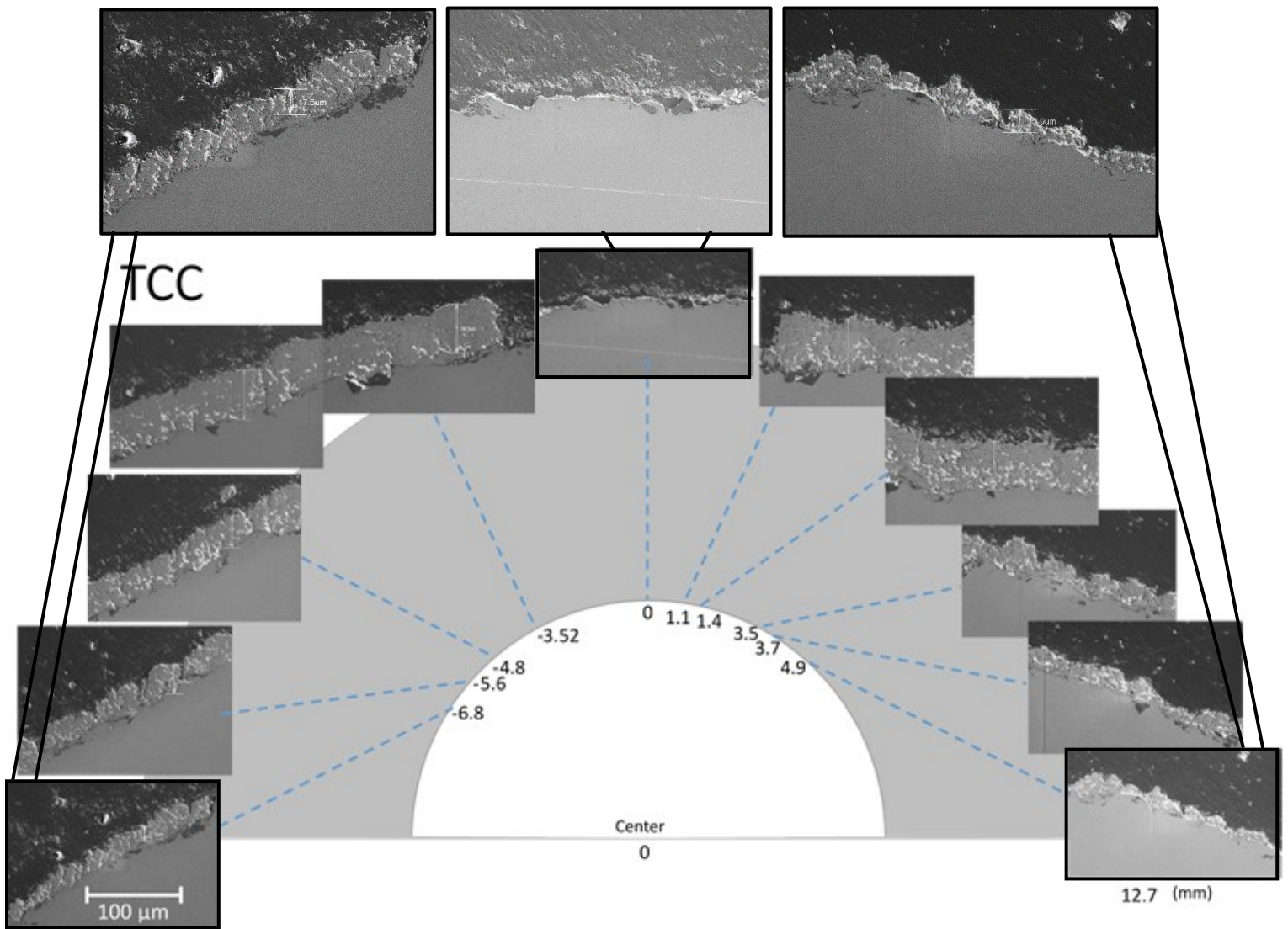


Figure 42 - Thick Coarse Cylinder (TCC) cross-section SEM images

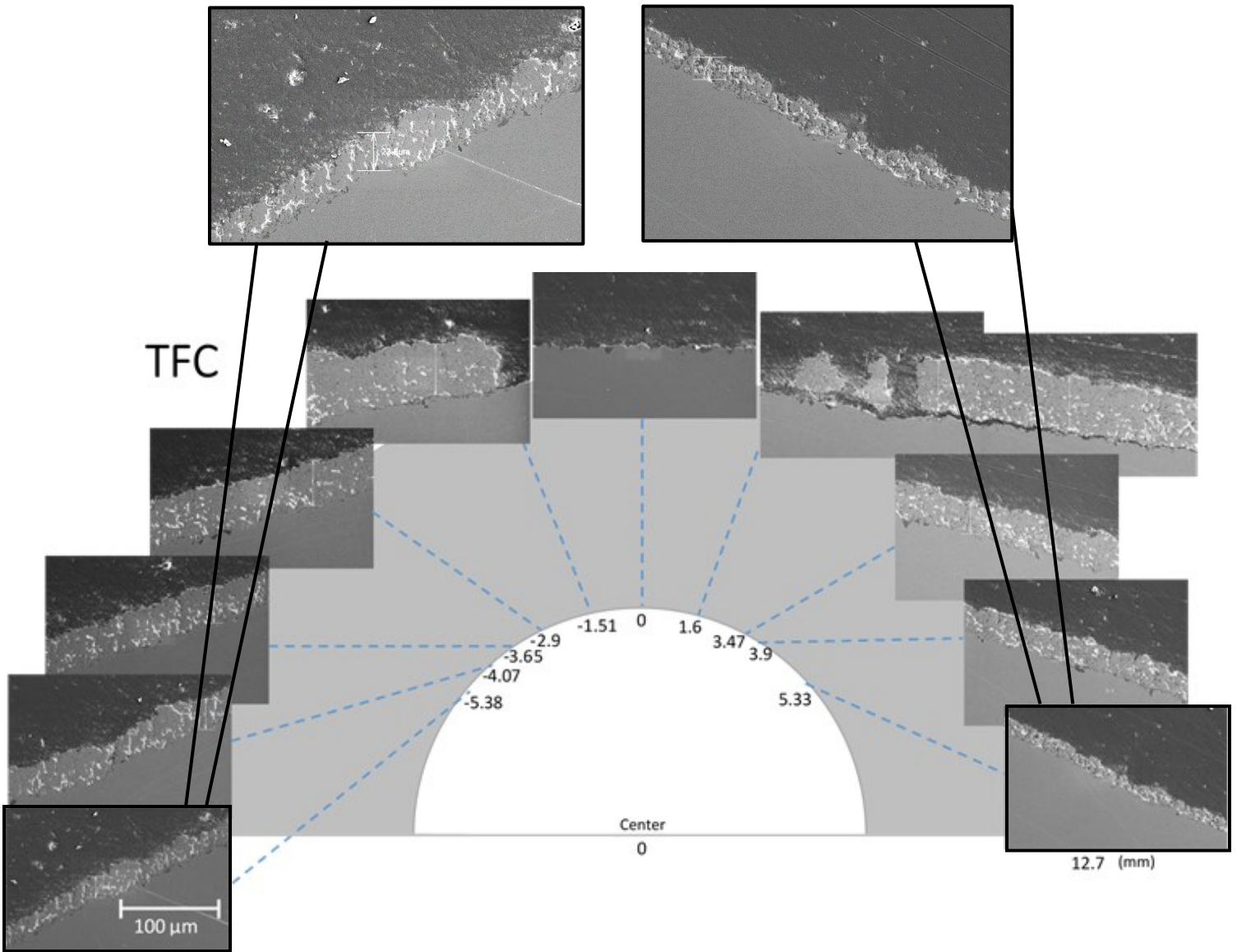


Figure 43 - Thick Fine Cylinder (TFC) cross-section SEM images

The polished cylinder sample (TPC) indicated more delamination than the other cylinder samples and some vertical cracks can be seen within the bottom side of the coating (Figure 44). Columns are present in the end of the footprint in both bottom and top side of the coating. Shadow effect is less prominent in this coating.

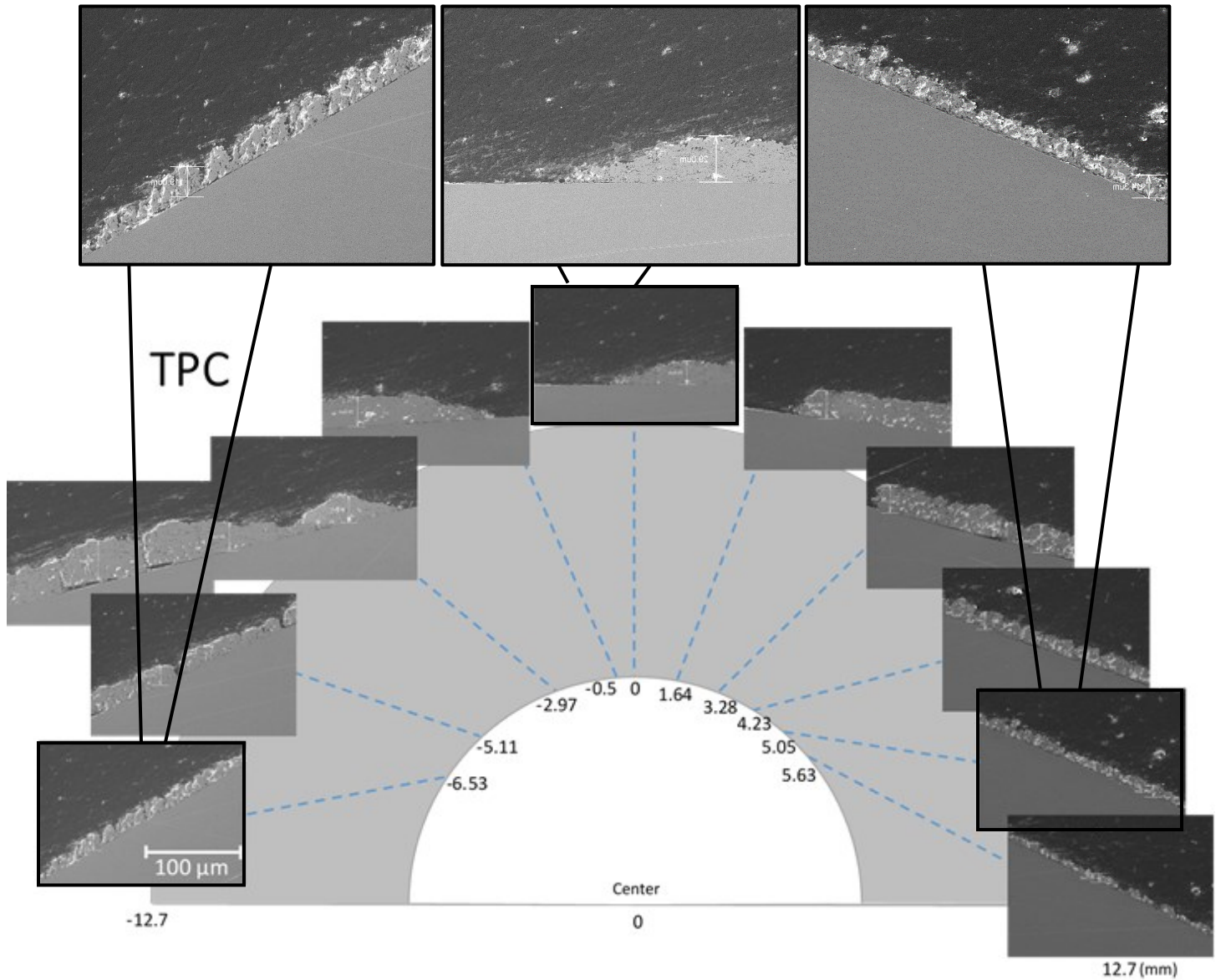


Figure 44 - Thick Polished Cylinder (TPC) cross-section SEM images

The thick cylinder had delamination in all the samples. Table 8 brings the thickness measured and Figure 45 a) shows that for TFC and TCC, there is no coating in the center of the substrate. TPC presented a thinner coating in the center due to delamination as well.

Table 8 – Thickness of Thick Cylinder samples in different positions

THICKNESS						
Position	TPC		TFC		TCC	
	Mean	St dev	Mean	St dev	Mean	St dev
-6.3	19.1	2.53	24.7	5.11	24.6	7.05
-5.1	23.3	3.53	27.7	4.61	30.7	9.16
-3	35.3	13.79	47.3	4.5	57.4	4.04
0	23.5	6.74				
1.6	34.4	1.32	56.9	5.75	55.4	5.79
3.4	31.8	3.03	37	2.73	25.2	12.02
3.8	20.4	2.14	31.7	2.48	17.8	5.2
4.8	14.5	2.07	14.3	4.71	15.1	6.89

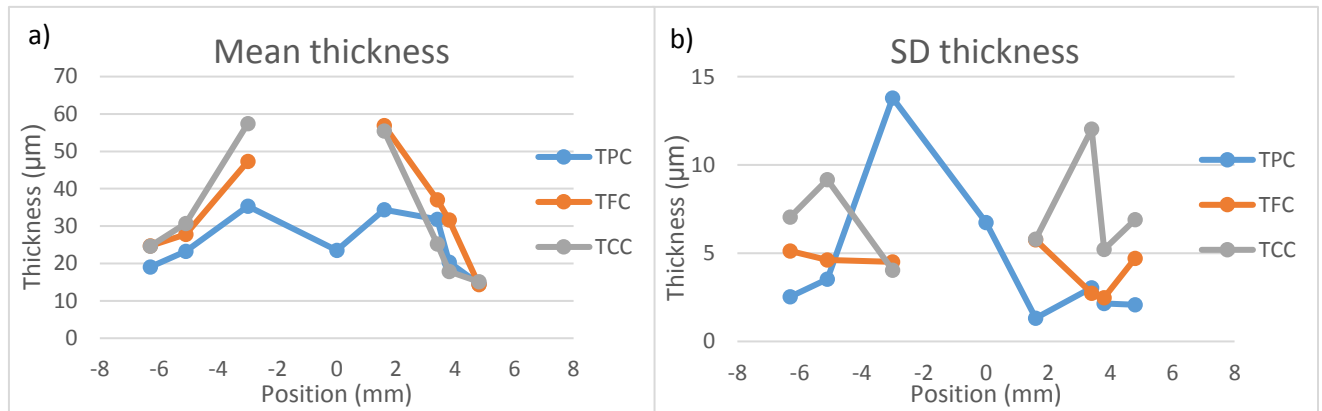


Figure 45 - a) Thickness measured for Thick Cylinder samples, and b) variation of thickness for Thick Cylinder samples

For these samples it is not possible to say that the thicker part of the coating was located at the center of the substrate due to the coating delamination. Figure 45 b) shows a high variation of coating thickness for TPC, due to delamination. The variation is also elevated for TCC because of the strong shadow effect present in this coating.

TFC and TCC had a higher variation in the roughness after spraying due to delamination and to shadow effect in the end of coating footprint as shown in Figure 46 a):

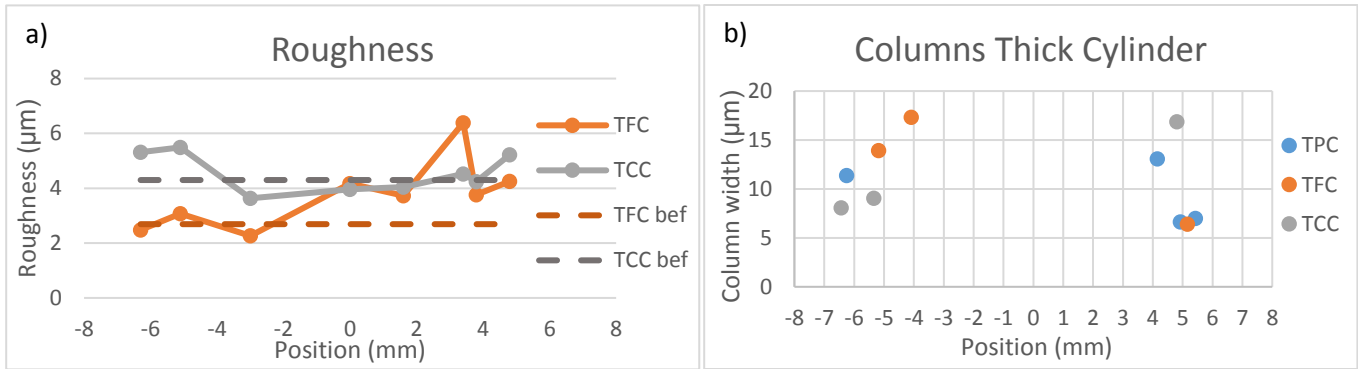


Figure 46 - a) roughness measured for Thick Cylinder samples, and b) columns width measured for Thick Cylinder samples

Columns were present in all the thick cylinder samples, on both top and bottom sides (Figure 46 b)). TFC and TCC presented more columns on the bottom side of the samples, meanwhile TPC presented more columns on the top side of the sample.

4.1.6 Thick rod samples

The rod samples also had delamination in all the samples. Columns are seen in the three samples as well. Once again, the shadow effect is stronger in the coarse sample and lighter in the fine and polished samples. Figure 47, Figure 48 and Figure 49 show TCR, TFR and TPR coatings respectively.

In TCR, the coating was detached from the substrate in the center, but did not break out. On the other hand, in TFR, there is not coating in the center of the substrate due to delamination. Moreover, in TPR, the coating delaminated during spraying and some extra layers were deposited in the following passes, forming a thinner coating in some parts of the center of the substrate, and some voids without any coating attached.

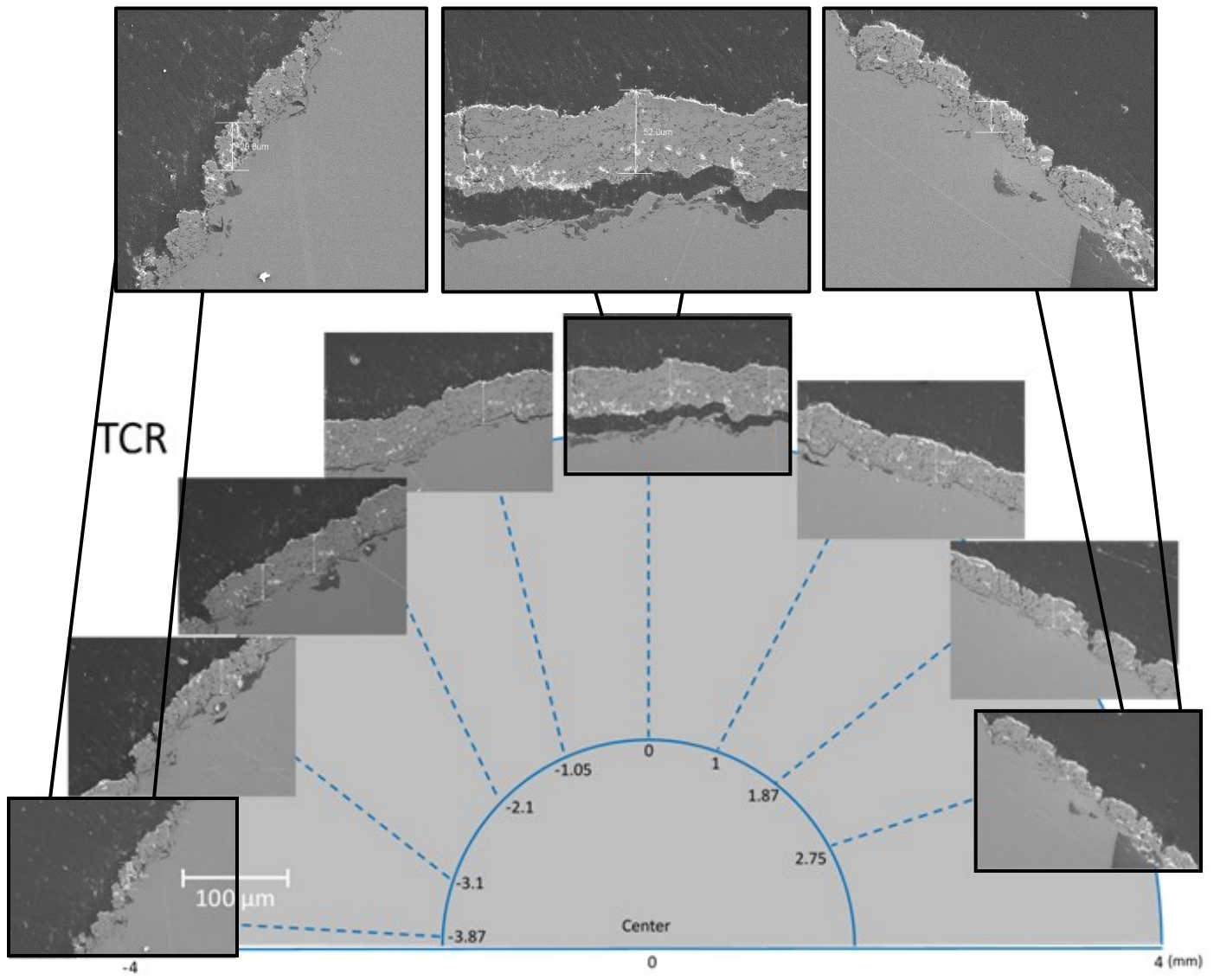


Figure 47 - Thick Coarse Rod (TCR) cross-section SEM images

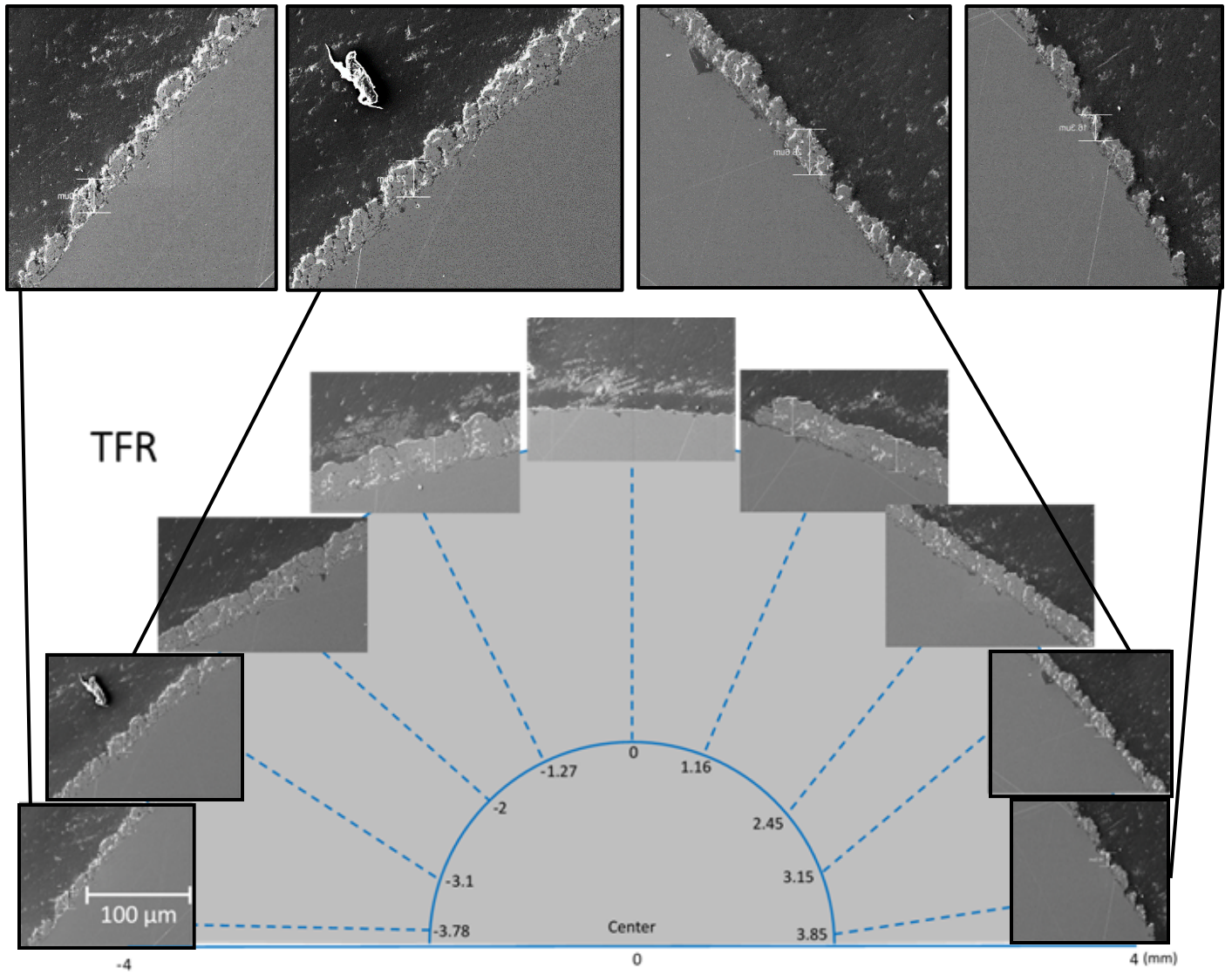


Figure 48 - Thick Fine Rod (TFR) cross-section SEM images

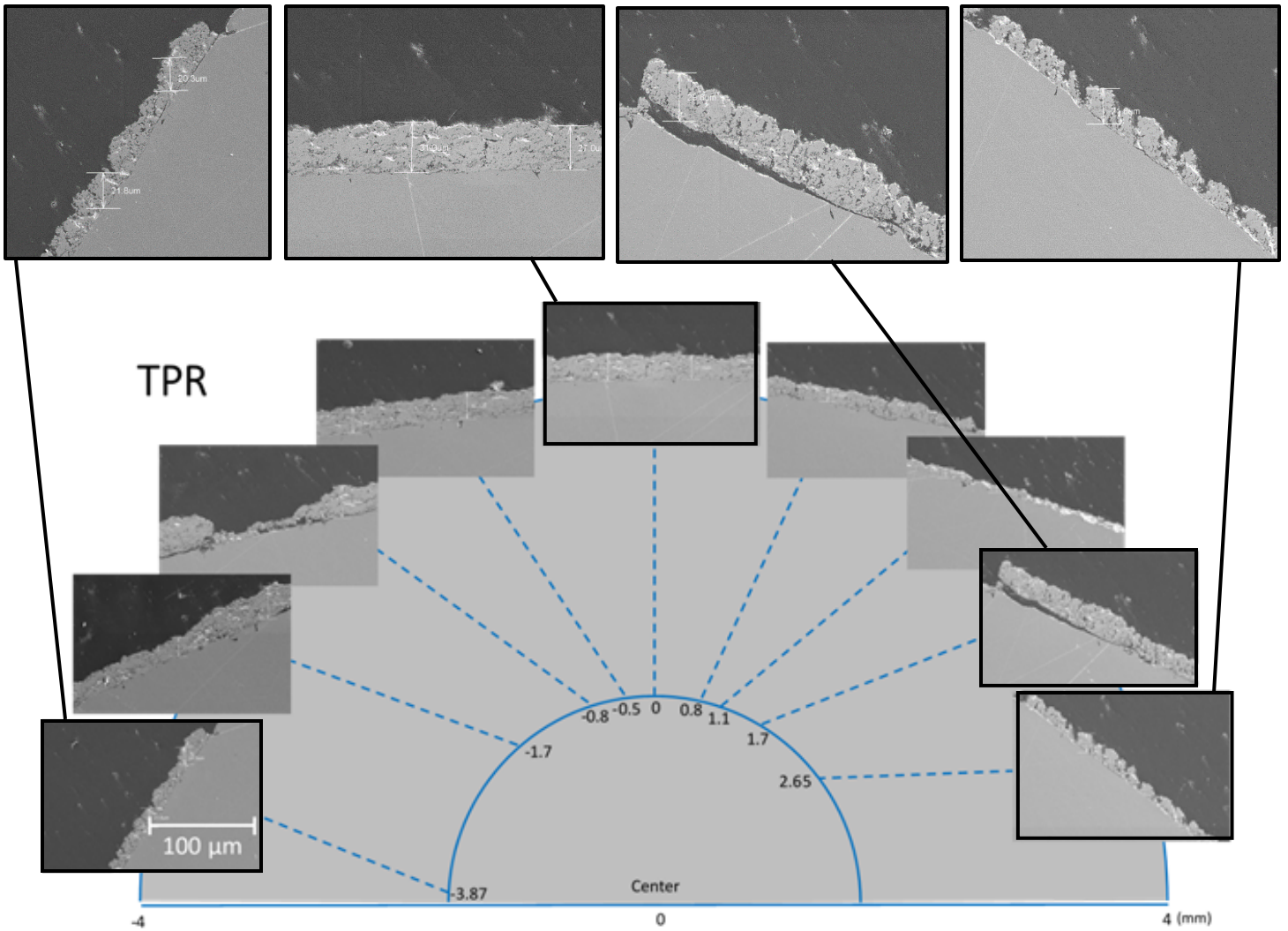


Figure 49 - Thick Polished Rod (TPR) cross-section SEM images

Table 9 shows the thickness measured. TCR had delamination, however, as seen in the SEM images, the coating did not break out of the sample. TFR had complete delamination in the center of the sample and TPR had delamination during spraying and some coating was built after delamination (Figure 50 a)). Figure 50 b) shows a big variation in the coating thickness for TPR due to delamination. On the other hand, TCR and TPR had a high variation on thickness on the top side of the sample due to shadow effect and columns.

Table 9 – Thickness of Thick Rod samples in different positions

THICKNESS						
Position	TPR		TFR		TCR	
	Mean	St dev	Mean	St dev	Mean	St dev
-3.8	15.8	2.11	16.3	1.24	15.5	3.32
-2.8	21.8	5.69	18.1	3.86	31.2	6.35
-1.6	25.2	4.06	37.9	7.13	45.1	5.92
-0.8	23.1	12.49	46.9	1.35	46.8	3.75
0	27.1	0.82			49.6	5.57
1	9.3	1.85	36.2	7.04	39.5	5.79
2	19.5	3.74	22.7	4.18	23.4	8.76
2.8	10.9	6.71	18.2	4.09	17.3	7.08

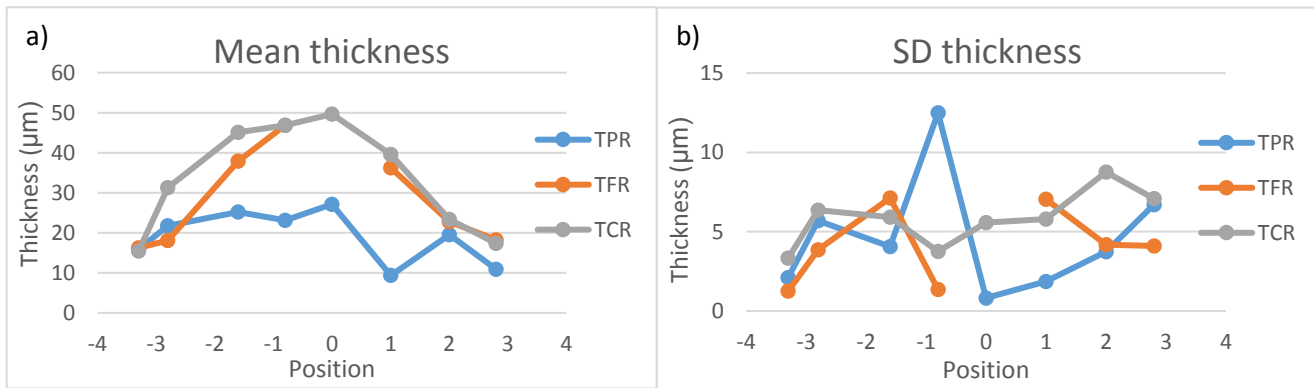


Figure 50 - a) Thickness measured for Thick Rod samples, and b) variation of thickness for Thick Rod samples

The roughness measured before and after spray can be seen in Figure 51 a). Due to delamination, TPR had a very different roughness after spraying. In addition, TFR and TCR remained close to the substrate roughness before spraying.

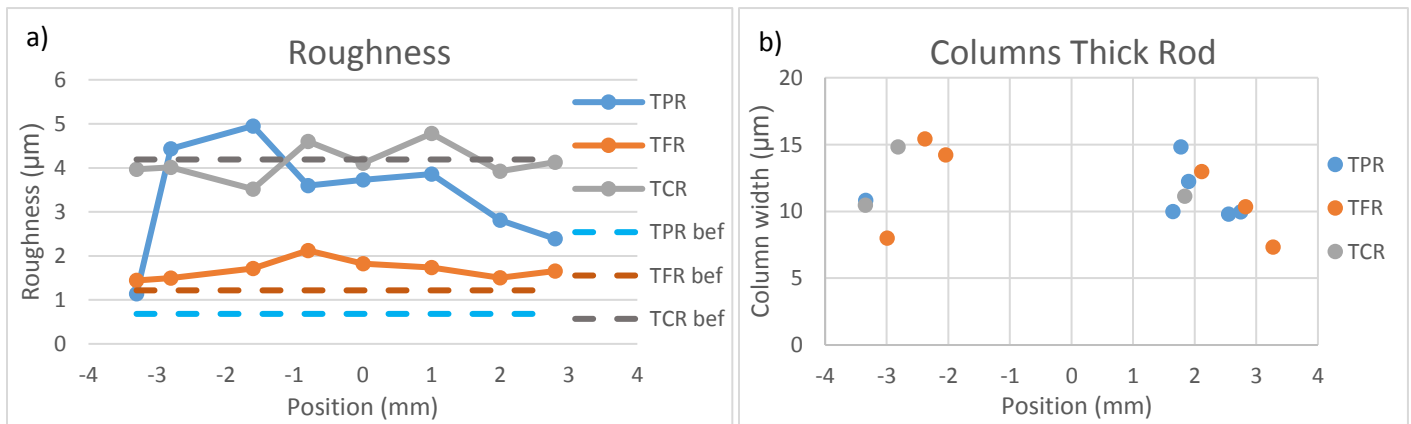


Figure 51 - a) Roughness measured for Thick Rod samples, and b) columns width measured for Thick Rod samples

Thick rod samples presented more columns than other geometries. As shown in Figure 51 b), all the samples formed columns on both top and bottom sides of the substrates.

4.2 Discussion

After the image analyses, some more specific observations can be made:

- It was observed that the center and bottom of substrate had a higher deposition, since the coatings were thicker at those locations.
- Flat samples also had thicker coatings than the other two shapes, indicating that in the other geometries, part of the particles might have followed the gases flow and did not impinge on the substrates.
- Columns are only present closer to the end of the coating footprints, indicating that they are formed by fine particles that follow the plasma flow. Perhaps, the angle which the particles are arriving to the substrate may also play a role in building the columnar structure.
- For the samples that presented columns, in general the columns have grown in an orientation parallel to the torch axis, except for 4PC.
- Substrate shape influences column growth, as seen in Figure 38, Figure 43 and Figure 48, for example. A higher amount of well-defined columns are seen in the rod sample, then in the cylinder, and lastly, less columns are present in the flat substrate.
- In the first series of samples, delamination occurred only in polished samples. For the second series of samples, due to higher thickness causing more stress in the center of deposition, delamination was present in all curved samples.

These observations can be compared to Pourang et al. [37] modeling results. Their findings showed a higher amount of coating material deposited on flat samples than on the curved ones. For that case, in a fixed time interval, particles hit the flat substrate surface 2.2 times more than the curved substrate surface. Higher deposition on flat substrates was also observed in these experimental results.

Moreover, the area of the coating in the samples cross-section was calculated. Figure 52 shows the estimated coatings cross-section area of the thick coatings. Considering that these coatings were sprayed with the exact same conditions, it can be observed that the shape of the substrate is influencing the amount of coating material been deposited. For the rod and cylinder samples, a higher amount of particles might have followed the plasma gases flow and did not impinge on the substrate.

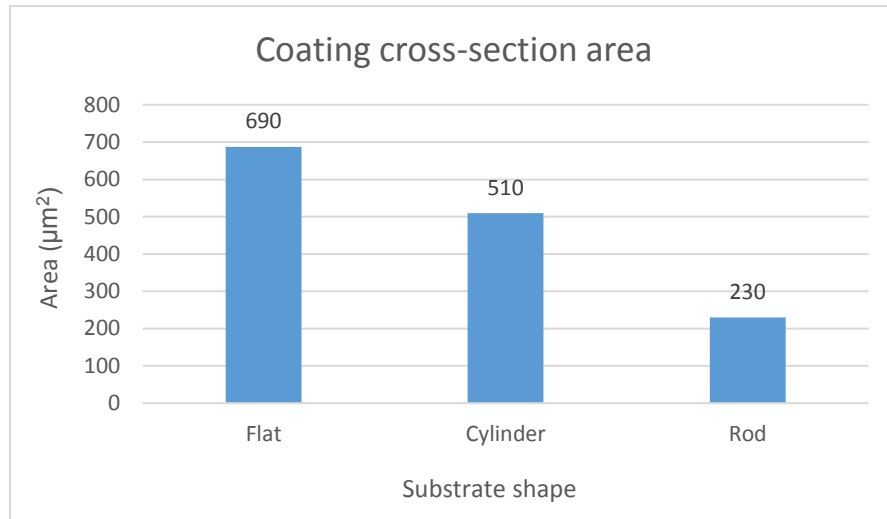


Figure 52 - Coating area in the cross-section of thick samples

These observations can be linked to Pourang et al. results [37] showing that the catch rate is higher on a flat substrate compared to a curved one. However, the difference in amount of coating material deposited from flat to cylinder samples in this work was only 25%. This can be explained by the position of the particle plume relative to the substrate position. In their case, the center of the deposition was not centered on the substrate, as shown in Figure 53 [37]. It is possible to see that most of the particles were arriving to the substrate at the torch axis location and above. On the other hand, in this work the center of deposition was located at the center of the substrate, having particles impinging on it both above and below the torch axis.

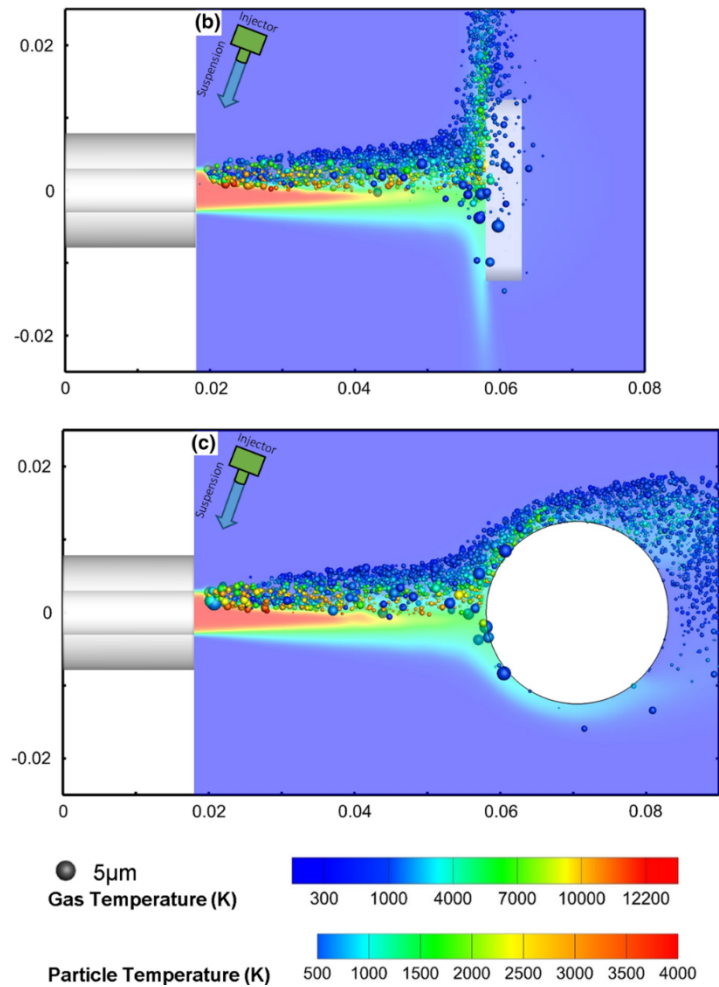


Figure 53 - Particles trajectory in flat and cylinder samples [37]

The decrease in the amount of coating material deposited on the rod samples was much larger. The coating footprints on flat and cylinder samples were wider than 10 mm as shown in Figure 40 a) and Figure 45 a). This represents more than the diameter of the rod samples, 8 mm. It is evident that much more particles have followed the gases flow trajectory and did not impinge on the rod substrate. This explains the 67% less coating material deposited on rod samples when compared to flat samples, and 55% when compared to cylinder samples.

The columns orientations was expected to be different. As the work conducted by Oberste-Berghaus et al. [38], the columns formed in the alumina coatings sprayed in a horizontal line above and below the torch exit where inclined towards the center of deposition (Figure 54).

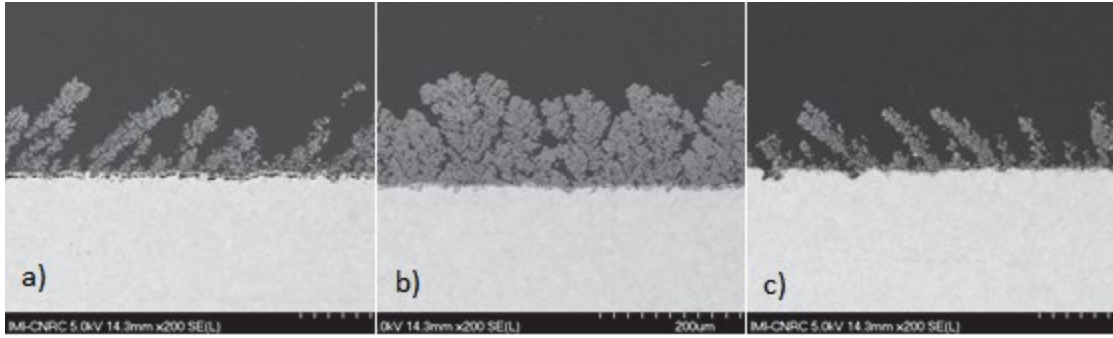


Figure 54 - Alumina coating structure at stagnation point flow close to the torch exit: a) below the jet, b) at the center, and c) above plasma jet [38]

The difference observed in this work and Oberste-Berghaus's might be due to the thickness of the coatings. The thickness of the coatings with columns inclined towards the center is much bigger than the ones sprayed during this work. It is believed that after more passes, getting to a thicker stage, the inclination of the columns would start occurring due to the shadow effect and the angle which the fine particles reach the substrate. Another reason could be the density of the particles sprayed. YSZ is almost 1.5 times denser than alumina. This factor might have helped those fine particles to follow the plasma gases flow more easily than in YSZ coatings.

A study performed by Kanouff et al. [39] analyzed coatings sprayed with an off-normal angle. A numerical model was validated with experimental results which showed that when the particles impinge on the substrate, a fraction of it splashes off the substrate and is redeposited with a small direction angle. This fraction is called overspray. Figure 55 shows the digitized data for the cross-section of the substrate sprayed.

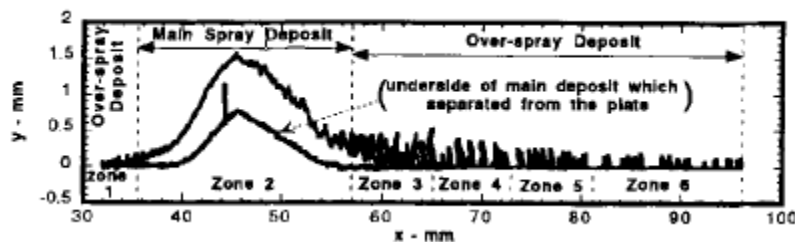


Figure 55 - Digitized data for the substrate cross-section [39]

It is possible to see that on the spray jet area, the coating is thicker and without much variation in the roughness. However, the over-sprayed portion shows a columnar structure. Their explanation is that the material was deposited with a very small direction angle. Figure 56 shows the micrograph of the columnar structure in the over-sprayed zones. They have concluded that

the over-sprayed material impacted the substrate at angles smaller than 8° , even though the angle of the columns is greater.

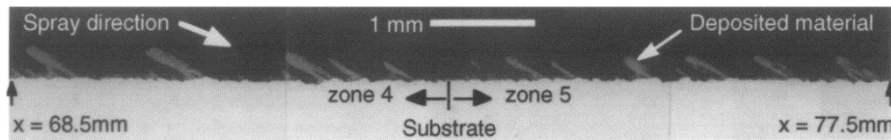


Figure 56 - Micrograph of the coating in the over-sprayed area [39]

The results presented by Kanouff et al. (1998) can be related to the results of this study. In all the samples, the center of deposition presented thicker coatings and less roughness variation, except when there was delamination. The columns were also formed in the periphery of the coatings. As seen in their work, the particles forming columnar structure are also believed to arrive to the substrate with a small direction angle. However, the orientation of the columns does not follow the same angle of impact. Figure 57 shows the schematic of the geometry of curved substrates and particles possible trajectories. The same situation is seen in Kanouff's results.

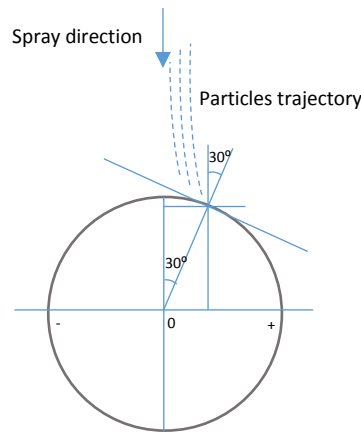


Figure 57 - Schematic curved substrate and particles possible trajectories before impact

Finally, as already seen, the columnar structure was present only in the periphery of the coatings, while the center of deposition presented a denser microstructure with two zones: fully melted areas (I) and sintered grain areas (II), as shown in the study performed by Carpio et al. [32].

5. Conclusions and Future work

An experimental research was performed to investigate if the geometry of a curved substrate and/or its surface roughness affect the coating microstructure. Several samples with three different shapes and three roughness were sprayed divided in two batches. The spraying strategy used was one straight line horizontally in the center of the substrate. First batch was sprayed with 50 passages in front of the substrates. The second batch was sprayed in 100 passes in order to increase the thickness of the coatings and observe further development of the structures. The suspension used was YSZ 20 wt.% in ethanol with radial injection.

It is still not possible to accurately measure in-flight particles' size, temperature and velocity what makes it harder to compare with other experimental results. The image analyses of the SPS coatings showed columns in the periphery of the coatings and denser two zones structures in the center of the substrates. Thickness of the coatings was found different for identical spray conditions, but different substrate shapes. With these observations, it is possible to conclude that, for this work, the substrate shape influences the amount of coating deposited, and as the radius of the curvature decreases, the amount of coating material deposited also decreases.

Additionally, the columns seem to be formed by very fine particles that follow the plasma gases flow and change direction in the stagnation region, impinging on the substrate off center of the torch exit. After some passes, due to shadow effect, these columns become more evident. The shape of the substrate also influences in column formation. The curved substrates had a more rapidly column growth, with better defined columns. As the radius of curvature decreased, more columns were formed. This might be due to the particles impacting angle at a specific location.

The surface roughness also plays a role in forming columnar structure. The shadow effect is said to be actively affecting the columns formation, therefore, the increase in the roughness will also increase the shadow effect, favoring the columnar growth. Moreover, as seen in the results, polished samples are more likely to delaminate.

For future work, a full raster to coat the entire substrate will be interesting to spray, in order to see the effect of the overlapping beads and how the columnar structure would be developed. Furthermore, another interesting experimental work would be the inside part of a cylinder. The curvatures considered in this work were on the convex side. However, the concave side will have a much different effect on the plasma gases flow and, consequently, in the particles trajectory.

Additionally, in modeling, a more detailed comparison with the numerical model, for example on angle of impact of the particles as a function of the distance from the center of the deposition. Finally, this current work can be extremely useful for validating coating build-up models.

References

- [1] D. E. Crawmer, "Thermal Spray Processes," in *Thermal Spray Technology. Vol 5A, ASM Handbook*, ASM International, 2013, pp. 33-53.
- [2] P. Fauchais, G. Montavon, R. S. Lima and B. R. Marple, "Engineering a new class of thermal spray nano-based microstructures from agglomerated," *JOURNAL OF PHYSICS D: APPLIED PHYSICS*, vol. 44, pp. 1-53, 2011.
- [3] N. P. Padture, M. Gell and E. H. Jordan, "Thermal Barrier Coatings for Gas-Turbine Applications," *Science*, vol. 296, pp. 280-284, 2002.
- [4] G. Mauer, M. O. Jarligo, D. E. Mack and R. Vassen, "Plasma-Sprayed Thermal Barrier Coatings: New Materials, Processing Issues, and Solutions," *Journal of Thermal Spray Technology*, vol. 22, no. 5, pp. 646-658, 2013.
- [5] B. Bernard, A. Quet, L. Bianchi, V. Schick, A. Joulia, A. Malie and B. Remy, "Effect of Suspension Plasma-Sprayed YSZ Columnar Microstructure and Bond Coat Surface Preparation on Thermal Barrier Coating Properties," *Journal of Thermal Spray Technology*, vol. 26, p. 1025–1037, 2017.
- [6] E. Bakan and R. Vassen, "Ceramic Top Coats of Plasma-Sprayed Thermal Barrier Coatings: Materials, Processes, and Properties," *Journal of Thermal Spray Technology*, vol. 26, p. 992–1010, 2017.
- [7] P. Fauchais, J. Heberlein and M. Boulos, *Thermal Spray Fundamentals*, New York: Springer, 2014.
- [8] N. Curry, K. VanEvery, T. Snyder and N. Markocsan, "Thermal Conductivity Analysis and Lifetime Testing of Suspension Plasma-Sprayed Thermal Barrier Coatings," *Journal of Thermal Spray Technology*, vol. 4, pp. 630-650, 2014.
- [9] R. Vaßen, H. Kaßner, G. Mauer and D. Stover, "Suspension Plasma Spraying: Process Characteristics and Applications," *Journal of Thermal Spray Technology*, vol. 19, no. 1-2, p. 219–225, 2010.
- [10] Z. Zou, J. Donoghue, N. Curry, L. Yang, F. Guo, P. Nylén, X. Zhao and P. Xiao, "A comparative study on the performance of suspension plasma sprayed thermal barrier coatings with different bond coat systems," *Surface & Coatings Technology*, vol. 275, pp. 276-282, 2015.
- [11] P. Fauchais, J.-F. Coudert, R. Etchart-Salas and G. Montavon, "Operating parameters for suspension and solution plasma-spray coatings," *Surface & Coatings Technology*, vol. 202, p. 4309–4317, 2008.
- [12] P. Fauchais, R. Etchart-Salas, V. Rat, J.-F. Coudert, N. Caron and K. Wittmann-Teneze, "Parameters controlling liquid plasma spraying: solutions, sols, or suspensions," *Journal of Thermal Spray Technology*, vol. 17, no. 1, p. 31–59, 2008.

- [13] P. Fauchais and G. Montavon, "Latest Developments in Suspension and Liquid Precursor Thermal Spraying," *Journal of Thermal Spray Technology*, vol. 19, no. 1-2, p. 226–239, 2010.
- [14] M. Aghasibeig, *Engineered Thermally Sprayed Electrodes for Hydrogen Production by Alkaline Water Electrolysis*, Montreal: Concordia University, 2015.
- [15] P. Fauchais, M. Vardelle, A. Vardelle and S. Goutier, "What Do We Know, What are the Current Limitations of Suspension Plasma Spraying?," *Journal of Thermal Spray Technology*, vol. 24, no. 7, pp. 1120-1129, 2015.
- [16] D. E. Crawmer, "Process Control and Control Equipment," in *Thermal Spray Technology. Vol 5A, ASM Handbook*, ASM International, 2013, p. 65–75.
- [17] L. Pawlowski, "Suspension and solution thermal spray coatings," *Surface & Coatings Technology*, vol. 203, pp. 2807-2829, 2009.
- [18] O. Marchand, L. Girardot, M. P. Planche, P. Bertrand, Y. Bailly and G. Bertrand, "An insight into suspension plasma spray: injection of the suspension and its interaction with the plasma," *Journal of Thermal Spray Technology*, vol. 20, no. 6, p. 1310–1320, 2011.
- [19] D. Damiani, D. Tarlet and E. Meillot, "A Particle-Tracking-Velocimetry (PTV) Investigation of Liquid Injection in a DC Plasma Jet," *Journal of Thermal Spray Technology*, vol. 23, no. 3, pp. 341-353, 2014.
- [20] L. Pawlowski, "Finely grained nanometric and submicrometric coatings by thermal spraying: A review," *Surface & Coatings Technology*, vol. 202, p. 4318–4328, 2008.
- [21] P. Fauchais, M. Vardelle, S. Goutier and A. Vardelle, "Specific Measurements of In-Flight Droplet and Particle Behavior and Coating Microstructure in Suspension and Solution Plasma Spraying," *Journal of Thermal Spray Technology*, 2015.
- [22] A. Joulia, W. Duarte, S. Goutier, A. Vardelle and S. Rossignol, "Tailoring the Spray Conditions for Suspension Plasma Spraying," *Journal of Thermal Spray Technology*, vol. 24, no. 1-2, pp. 24-29, 2014.
- [23] M. Jadidi, M. Mousavi, S. Moghtadernejad and A. Dolatabadi, "A Three-Dimensional Analysis of the Suspension Plasma Spray Impinging on a Flat Substrate," *Journal of Thermal Spray Technology*, vol. 24, no. 1-2, pp. 11-23, 2015.
- [24] A. Ganvir, N. Curry, N. Markocsan, P. Nylen, S. Joshi, M. Vilemova and Z. Pala, "Influence of Microstructure on Thermal Properties of Axial Suspension Plasma-Sprayed YSZ Thermal Barrier Coatings," *Journal of Thermal Spray Technology*, vol. 25, no. 1-2, pp. 202-212, 2016.
- [25] K. VanEvery, M. J. Kranr, R. W. Trice, H. Wang, W. Porter, M. Besser, D. Sordelet, J. Ilavsky and J. Almer, "Column Formation in Suspension Plasma-Sprayed Coatings and Resultant Thermal Properties," *Journal of Thermal Spray Technology*, vol. 20, no. 4, pp. 817-828, 2011.

- [26] A. Ganvir, N. Curry, S. Bjorklund, N. Markocsan and P. Nylén, "Characterization of Microstructure and Thermal Properties of YSZ Coatings Obtained by Axial Suspension Plasma Spraying (ASPS)," *Journal of Thermal Spray Technology*, vol. 24, no. 7, pp. 1195-1204, 2015.
- [27] W. Riggs, D. Rucker and K. Couch, "Testing of Coatings," in *Thermal Spray Technology*, ASM International, 2013, pp. 214-237.
- [28] L. Pawlowski, *The Science and Engineering of Thermal Spray Coatings*, Wiley, 2008.
- [29] A. Macwan, M. Marr, O. Kesler and D. L. Chen, "Microstructure, hardness, and fracture toughness of suspension plasma sprayed yttria-stabilized zirconia electrolytes on stainless steel substrates," *Thin Solid Films*, pp. 23-28, 2014.
- [30] E. Meillot, D. Damiani, S. Vincent, C. Caruyer and J. P. Caltagirone, "Analysis by modeling of plasma flow interactions with liquid injection," *Surface & Coatings Technology*, vol. 220, pp. 149-156, 2013.
- [31] N. Curry, K. VanEvery, T. Snyder and S. Bjorklund, "Performance Testing of Suspension Plasma Sprayed Thermal Barrier Coatings Produced with Varied Suspension Parameters," *Coatings*, pp. 338-356, 2015.
- [32] P. Carpio, E. Bannier, M. Salvador, A. Borrell, R. Moreno and E. Sanchez, "Effect of particle size distribution of suspension feedstock on the microstructure and mechanical properties of suspension plasma spraying YSZ coatings," *Surface & Coatings Technology*, pp. 293-297, 2014.
- [33] F. Jabbari, M. Jadidi, R. Wuthrich and A. Dolatabadi, "A Numerical Study of Suspension Injection in Plasma-Spraying Process," *Journal of Thermal Spray Technology*, vol. 23, no. 1-2, pp. 3-13, 2013.
- [34] N. Curry, Z. Tang, N. Markocsan and P. Nylén, "Influence of bond coat surface roughness on the structure of axial suspension plasma spray thermal barrier coatings - Thermal and lifetime performance," *Surface & Coatings Technology*, pp. 15-23, 2014.
- [35] P. Sokolowski, S. Kozerski, L. Pawlowski and A. Ambroziak, "The key process parameters influencing formation of columnar microstructure in suspension plasma sprayed zirconia coatings," *Surface & Coatings Technology*, pp. 97-106, 2014.
- [36] P. Sokolowski, L. Pawlowski, D. Dietrich, T. Lampke and D. Jech, "Advanced Microscopic Study of Suspension Plasma-Sprayed Zirconia Coatings with Different Microstructures," *Journal of Thermal Spray Technology*, vol. 25, no. 1-2, pp. 94-104, 2016.
- [37] K. Pourang, C. Moreau and A. Dolatabadi, "Effect of Substrate and its Shape on in-Flight Particle Characteristics in Suspension Plasma Spraying," *Journal of Thermal Spray Technology*, vol. 25, no. 1-2, pp. 44-54, 2016.

- [38] J. Oberste-Berghaus, S. Bouaricha, J. G. Legoux and C. Moreau, "Injection conditions and in-flight particle states in suspension plasma spraying of alumina and zirconia nano-ceramics," in *Thermal Spray Conference*, Basel, 2005.
- [39] M. P. Kanouff, R. A. Neiser and T. J. Roemer, "Surface Roughness of Thermal Spray Coatings Made with Off-Normal Spray Angles," *Journal of Thermal Spray Technology*, vol. 7, no. 2, pp. 219-228, 1998.